67

Compartmentalization Evaluated to Explain Discrepancies Calculating Cartilage Fixed Charge Density

by

Arun Mammen Thomas

S.B. Massachusetts Institute of Technology
Cambridge, Massachusetts (1995)

Submitted to the Department of Electrical Engineering and Computer Science in Partial Fulfillment of the Requirements for the Degree of

Master of Engineering in Electrical Engineering and Computer Science

at the

MASSACHUSETTS INSTITUTE OF TECHNOLOGY

June 1998
[September, 1998]

Author: _____
Department of Electrical Engineering and Computer Science
May 26, 1998

Certified by: _____
Martha L. Gray
Thesis Supervisor

Accepted by: _____
Arthur C. Smith
Chairman, Department Committee on Graduate Theses

Eng

Evaluation of Compartmentalization as an Explanation of Discrepancies Calculating Fixed Charge Density in Cartilage

by
Arun Mammen Thomas

Submitted to the Department of Electrical Engineering and Computer Science
June 30, 1998
In Partial Fulfillment of the Requirements for the Degree of
Master of Engineering in Electrical Engineering and Computer Science

ABSTRACT

Recent studies on methods of detecting the early onset of arthritic cartilage degradation using NMR-based techniques have shown that such detection is possible. The use of sodium NMR observations, along with an ideal Donnan single compartment model of cartilage, has already been validated as a means of measuring cartilage fixed charge density - a known indicator of cartilage condition. Similar calculations of fixed charge density from proton (in the presence of gadopentetate) NMR observations and the same model were highly correlated with, but 50% below, values derived from sodium NMR. Maroudas had previously shown the water content of cartilage to be divided with a roughly 30:70 ratio between two physiologically distinct regions. The first of these regions, within cartilage collagen fibrils, is electroneutral, with most of the tissue fixed charge, in the form of chondroitin sulfate, being concentrated in the remainder of the tissue, the second region. The existence of two compartments, with different associated fixed charge densities, is shown, by spreadsheet computations and analysis of previously published data, to be a possible reason for the observed 50% discrepancy. High-concentration chondroitin sulfate solutions within dialysis tubing bags were equilibrated in solutions containing sodium and gadopentetate ions. This solution/tubing apparatus mimicked an ideal Donnan single compartment. MR measurements of the amounts of the two ions and calculations of fixed charge density in the solutions based on the measurements yielded the same 50% factor. Since this artificial model did not include any collagen, there were no compartmentalization effects due to structural factors. A similar single-compartment was done using a non-ionic contrast agent to test for steric exclusion based compartmentalization. Although MR measurements revealed a discrepancy in contrast agent distribution, the discrepancy was exactly opposite what should have been observed had steric exclusion been a factor. In summary, it seemed clear that compartmentalization of water (from either cartilage structure or from steric exclusion) was not primarily responsible for the observed 50% discrepancy. Another explanation must be found.

Thesis Supervisors:

Deborah Burstein, Ph.D.
Associate Professor of Radiology
Beth-Israel Hospital
Harvard Medical School

Martha L. Gray, Ph.D.
J.W. Kieckhefer Professor of Electrical Engineering
Department of Electrical Engineering and Computer Science
MIT and Harvard-MIT Division of Health Science and Technology

Table of Contents

List of Figures

List of Tables

Chapter 1: Introduction

Articular cartilage is a connective tissue found covering the surfaces of the bones in a joint. It provides a lubricated surface to permit smooth motion, and serves to harmlessly transfer load across the joint. Osteoarthritis is a degenerative disease of cartilage progressing from inflammation to eventual destruction of the tissue. It affects millions of people around the world. The United States, in particular, has cause for concern as the baby-boom generation reaches the age groups found to be most affected by arthritis. A 1992 study [77] (based on U.S. data collected between 1970 and 1987) showed that over 55% of those over 70 years of age were afflicted with arthritis. This makes the disease the number one concern for the elderly. The same study showed, however, that the elderly are not the only ones affected by this disease.

Although arthritis only affects a mere 5% of the working age adults – those between 18 and 64 years of age – the percentages shield the actual impact of disease. In fact, over 9 million of the working age adults in the United States reported having arthritis, and 5.5 million found their activities limited by the disease. The study continued on to show that arthritis had an obvious detrimental effect on the labor participation rate of those afflicted.

Clearly, arthritis is a disease with great relevance to the concerns of the nation and, indeed, to the individuals of that nation. It is also a disease that is currently not well understood. Preventive methods are primarily focused on eliminating risk factors derived from an understanding of the function of cartilage at a mechanical rather than a molecular level [64]. Current methods of diagnosis are based very much on reports of subjective symptoms such as stiffness, swelling, fatigue, tenderness, pain, etc. A generally accepted

quantitative method for identifying the disease has yet to be established. Visualization procedures for arthritis suffer from similar problems. Historically, visualization was via radiographs, which permitted only an indirect and clumsy assessment of cartilage condition by examining the space between the bones at a joint. More recently, arthography and computed tomography permitted better visualization, but even these invasive techniques were unable to identify arthritis prior to the appearance of gross structural changes.

Magnetic resonance imaging (MRI), a visualization technique developed from nuclear magnetic resonance (NMR), is an even more recent arrival in the visualization field. It has met with considerable success imaging cartilage as several techniques now exist to enhance the MRI contrast between different types of tissue. (The delineation between the hard – bone – and soft – cartilage – tissues of joints is particularly good.) Work has even been done to show that changes in cartilage thickness can be visualized using MRI, permitting replacement of the more traditional radiographic images [63].

Recent efforts have focused using NMR and MRI as non-invasive tools to quantitatively diagnose arthritis by attempting to detect pathologic indications of the disease state. One of the early signs of osteoarthritis, is the loss of one type of material, proteoglycan, from the tissue. Venn and Maroudas [72] showed that arthritic cartilage shows a significant reduction in proteoglycans as compared to normal cartilage. A means of measuring the proteoglycan content of cartilage, therefore, would provide a direct measure of tissue health. MR methods for diagnosing arthritis have focused on just such early detection of changes in cartilage proteoglycan content by making use of specific properties of the compound. Lesperance et al [47] showed that NMR measurements of

sodium content of *in vitro* samples can lead to a quantitative determination of proteoglycan content. Bashir et al's work [7] made use of the same principles to demonstrate that proton NMR in the presence of a specific MR contrast agent, gadopentetate dimeglumine, could be used for the same purpose. Recent work has further established that MRI in the presence of gadopentetate dimeglumine can distinguish arthritic cartilage from healthy human tissue and has suggested that *in vivo* monitoring of proteoglycan is possible [5,6].

Strangely, although the technique established by Bashir et al succeeds in tracking proteoglycan content, simultaneous measurements with sodium NMR and proton NMR yield quantitative values that differ by roughly a factor of two [7]. The goal of this work is to explore one hypothesis explaining the nature of this factor.

Chapter 2: Essential Background

2.1 Cartilage Physiology

There are many different cartilaginous tissues in the body. Nevertheless, all forms of cartilage share a gross similarity in their composition. Cartilage is a mostly cell-free tissue. The endogenous cells, known as chondrocytes, take up only about three to five percent of the tissue volume. They do not take an active role in the biomechanical role that cartilage plays but maintain, via synthesis, secretion, and degradation, an extracellular matrix (ECM) to fill that role [31]. The ECM provides mechanical strength via two main routes – electrical interactions due to ionic groups, and mechanical interaction due to chemical bonds between the structural elements of the matrix [19].

This extracellular matrix, the main part of cartilage tissue, is made up of water (65-80% of wet weight), collagen (15-25%), proteoglycans (3-10%), and various other noncollagenous proteins and glycoproteins [51]. Considering the relatively low concentration of noncollagenous proteins and glycoproteins present, cartilage can, for some purposes, be considered primarily a two-phase mixture of porous but insoluble collagen fibers and a solution of water and proteoglycans [19]. Figure 2.1 is a cartoon sketch of a segment of cartilage incorporating the two main non-water components, collagen and proteoglycan. These two elements will be the focus of the remainder of this section.

The collagen building block is a triple helix of procollagen chains, which link to each other via disulfide bonds during synthesis. The resulting collagen monomers, molecules about 300nm long, are arranged into arrays in which individual monomers again cross-link, forming microfibrillar bundles (Figure 2.2). Assembly continues as

bundles link to each other, leading eventually to the formation of a mature collagen fibril. The final strand can be quite long (as much as 1μm) and can have a diameter ranging from 50 to 150nm depending on location [71]. This cross-linked collagen network provides the structural support upon which the ECM is built. It provides tensile strength, and limits swelling of the tissue from osmotic or hydrostatic pressures.

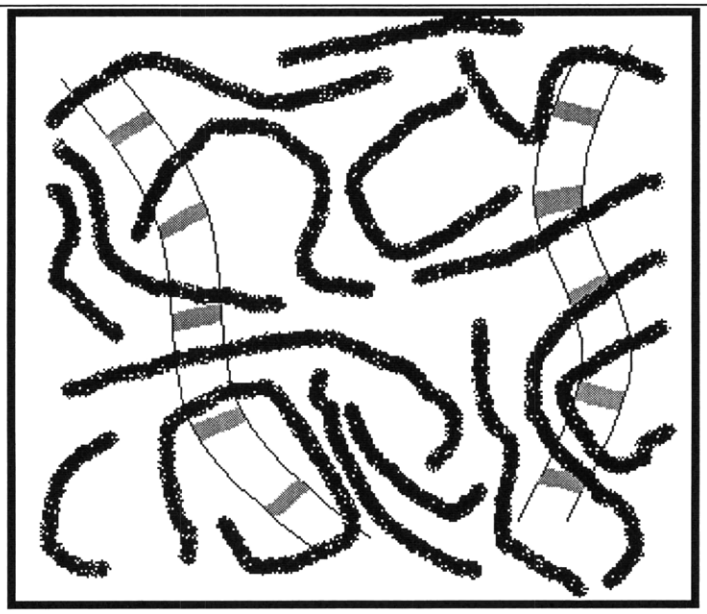

Figure 2.1: A cartoon sketch of cartilage structure depicting gray-banded collagen fibrils and black bottlebrush proteoglycans, the main constituents of cartilage. The white portions within the diagram should not be taken as empty, but rather, as filled with water. Also found in this space are noncollagenous proteins, glycoproteins, and chondrocytes (not depicted because they are unimportant for the purposes of this work).

It is useful to note that although collagen molecules have chemical groups which ionize at physiological pH, those which are positively charged (amino, NH^{+3}) are about equal in number to those which have a negative charge (carboxyl, COO^{-}). As a result, there is no net charge. This fact permits us to conclude below that collagen does not contribute to our MR measurements.

The other major non-water constituent of cartilage is the proteoglycans. The bottlebrush-like proteoglycans are usually found in large aggregates non-covalently inked

to hyaluronic acid chains. The binding of proteoglycan to acid is a complex process requiring a linking protein to join the binding region of the proteoglycan protein core to the acid. A proteoglycan is composed, as the name suggests, of a long protein core chain to which are attached other sugar compounds known as glycosaminoglycans (GAGs). In articular cartilage, these sugar compounds include disaccharide polymers, principally keratan sulfate (KS) and chondroitin sulfate (CS).

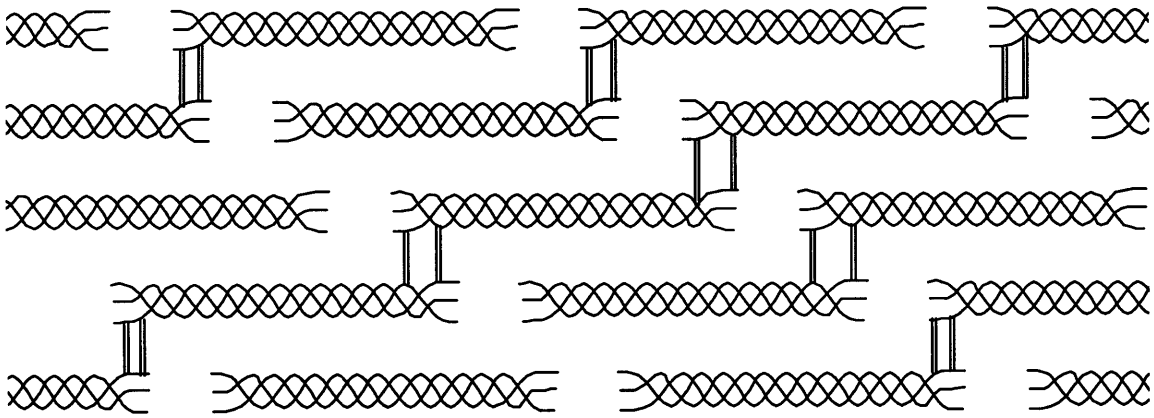

Figure 2.2: Collagen in the extracellular matrix. Three procollagen strands twine to form a triple helix, which cross-links with other similar strands to form a microfibrillar bundle. The microfibrillar bundles then undergo further cross-linking with other bundles to form higher order structures (larger fibrils and fibers).

Figure 2.3 shows a cartoon of one proteoglycan. A proteoglycan strand is known to have at least three different regions along the protein core [33]. One of these regions is particularly rich in bound keratin sulfate, while the other is rich in bound chondroitin sulfate. In general, the chondroitin sulfate is more plentiful not only because the CS polymers tend to be longer than the KS polymers, but also because the CS binding region is significantly larger, resulting in many more bound CS chains.

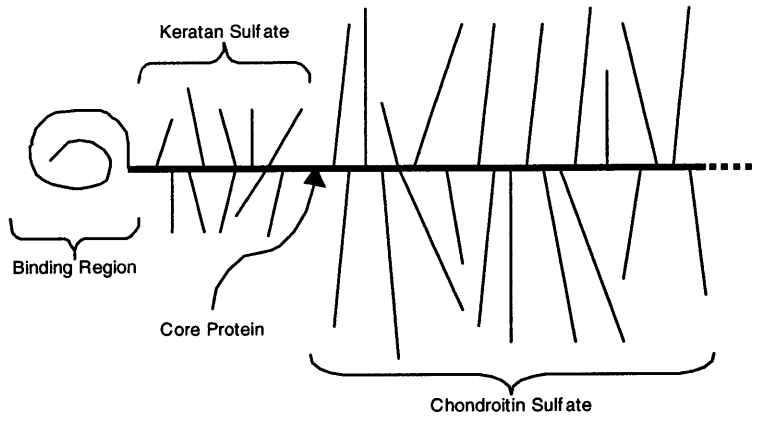

Figure 2.3: Cartoon of a proteoglycan molecule, the other major component of the cartilage extracellular matrix, marking the core protein and three distinct regions. For the purposes of this work, the focus will be primarily on the last region, the chondroitin sulfate, which is the main charge carrying material. Not shown here are the hyaluronic acid chains to which proteoglycans are bound, and the link proteins, which connect the binding region to the acid.

A structural diagram of the chondroitin sulfate monomer in both its neutral and ionized form is provided in Figure 2.4. At physiological pH, the disaccharide is ionized with both the carboxyl (COO^-) and sulfate (SO_3^-) groups negatively charged. Each

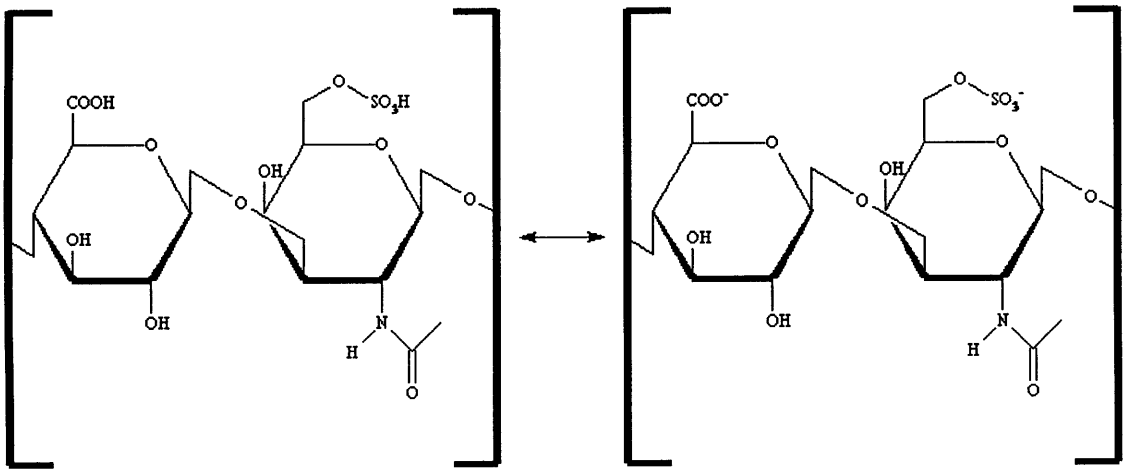

Figure 2.4: The structural diagram of the chondroitin sulfate monomer is shown here. At physiological pH, the monomer (MW = 459.39 g/mol) is ionized, with both the carboxyl and the sulfate groups maintaining a negative charge.

disaccharide, therefore, has a net -2 charge. Unlike unbound ions in the electrolytic fluid, which are free to diffuse in and out of the tissue, the charge on the chondroitin sulfate is

firmly "fixed" to the proteoglycans in the cartilage. As a result, the tissue is said to possess a fixed charge. In general, the concentration of fixed charge is referred to as the fixed charge density – FCD. (Although keratan sulfate has not been described specifically, it too is negatively charged at physiological pH – though only with a -1 charge per disaccharide [12] – contributing a component to the fixed charge density of cartilage.) The proteoglycans, because of their charge, become responsible for much of the stiffness and resilience of cartilage.

2.2 Donnan Based Derivation of FCD

The association of fixed charge with the proteoglycans on cartilage suggests that accurate determination of fixed charge density might act as a useful measure of the amount of proteoglycan in the tissue. (As has been noted previously, loss of proteoglycans is one of the early signs of the onset of arthritis.) One method of determining FCD, to be described here, makes use of measurements of mobile ion concentrations.

The presence of the fixed charge within the cartilage attracts mobile ions of opposite charge (counter-ions) and repels mobile ions of similar charge (co-ions). Therefore, although the tissue as a whole – solid and fluid components – has no net charge, an unequal distribution of mobile ions is set up between the tissue fluid and the external solution – which has no fixed charge. Since positive cations are preferentially attracted to the tissue while negative anions are repelled, the buildup of mobile charges sets up an electrical potential (the Donnan electrical potential) across the interface of the external solution and the cartilage. Distribution of ions obeys the Donnan equilibrium equation [51], which relates ion concentrations to the Donnan potential.

The ideal Donnan assumption states that electrolyte activity coefficients for ions are the same both in external solution and within any charged material, or, equivalently, that the ratio of electrolyte activities in external solution to electrolyte activities in charged material is equal to the ration of concentrations. This assumption, combined with some other approximations [30], leads to the following general expression:

$$\left(\frac{\overline{C}_i}{C_i}\right)^{1/Z_i} = e^{-\frac{F\Delta\Phi}{RT}}$$

Equation 2.1

where

$\overline{C}_i \equiv$ concentration of species i in charged material

$C_i \equiv$ concentration of species i in external solution

$Z_i \equiv$ charge on species i

$T \equiv$ temperature

$\Delta\Phi \equiv$ Donnan potential

$F \equiv$ Faraday's constant

$R \equiv$ ideal gas constant

This relationship tells us that, at equilibrium, which implies no net flux of ions, given a constant temperature, the ratio of concentrations of any species of ion within and without a charged material is fixed to a constant value.

Another useful generalization deals with bulk electroneutrality. On a macroscopic scale, any given volume must satisfy electroneutrality, the sum of all the positive and negative charges within the volume must be zero. The following equations express this statement for two regions; the interior of a charged material, and the external solution.

$$\sum_i \bar{z}_i \bar{c}_i + \mathrm{FCD} = 0$$

Equation 2.2

$$\sum_i z_i c_i = 0$$

Equation 2.3

Given these relationships, consider a sample of cartilage equilibrated in a solution with a relatively high concentration of NaCl (Na^+ and Cl^-), and much smaller concentrations of other minor ions (PO^{-3}, CO^{-3}, H^+, Gd-DTPA^{-2}). Applying Equation 2.1 to some of the ions results in the expression below.

$$\frac{\bar{c}_{Na^+}}{c_{Na^+}} = \frac{c_{Cl^-}}{\bar{c}_{Cl^-}} = \left(\frac{c_{Gd\text{-}DTPA^{-2}}}{\bar{c}_{Gd\text{-}DTPA^{-2}}} \right)^{1/2}$$

Equation 2.4

This expression could be further extended to incorporate all the other ions present as well. The Gd-DTPA^{-2} ion was chosen here as an example for reasons that will become clear later in this work.

Application of Equation 2.2 and Equation 2.3 requires a little more thought. In general, it is difficult to be absolutely sure exactly which ions are present in solution. Certainly, the external solution surrounding cartilage *in vivo* contains a whole melange of ions which differ to some extent depending on the individual in question. A key approximation, however, makes these two equations simpler. The choice is to approximate as equal to zero the concentrations of those ions which are present only at relatively low concentrations. In the human body, most fluids contain relatively large concentrations of NaCl, and a few other ions. The majority of the ions found are present only at very low concentrations. For the example described above, Equation 2.2 and Equation 2.3 simplify to the following:

$$\bar{c}_{Na^+} + \bar{c}_{Cl^-} + FCD = 0$$

Equation 2.5

$$c_{Na^+} + c_{Cl^-} = 0$$

Equation 2.6

Note that here, only the Na^+ and Cl^- ion need be considered, as all other ions are only present at relatively low concentrations.

Putting together Equation 2.4, Equation 2.5 and Equation 2.6, we can solve for fixed charge density in terms of the concentrations of various ions [7,47].

$$FCD = \frac{c_{Na^+}^2}{\bar{c}_{Na^+}} - \bar{c}_{Na^+} = \bar{c}_{Cl^-} - \frac{c_{Cl^-}^2}{\bar{c}_{Cl^-}} = c_{Na^+}\left(\sqrt{\frac{\bar{c}_{Gd\text{-}DTPA^{-2}}}{c_{Gd\text{-}DTPA^{-2}}}} - \sqrt{\frac{c_{Gd\text{-}DTPA^{-2}}}{\bar{c}_{Gd\text{-}DTPA^{-2}}}}\right)$$

Equation 2.7

Some method of measuring ion concentrations, therefore, could lead directly to a value for FCD. (Note, however, that measurements of anion concentrations are much more likely to lead to errors in the values calculated for FCD. Since anions are preferentially repelled from the negatively charged material, the actual concentrations present are quite low. A fixed magnitude measurement error, therefore, will correspond to a greater relative error for anions than for cations.) In the work described here, ion concentrations are measured using NMR, and these measured values used to evaluate fixed charge density.

2.3 Nuclear Magnetic Resonance (NMR)

The magnetic resonance techniques used for the various measurements in this work have all been adequately described in the literature [7,22,23,47]. Nevertheless, a certain minimum exploration of some of the fundamental ideas behind NMR is called for at this point. An excellent quick reference (with very helpful graphics) for understanding

the basics of NMR physics, can be found on the world wide web on the Sheffield Hallam University School of Science and Mathematics web server [1]. Another slightly more detailed and ornate, but perhaps more useful web reference can be found at http://www.cis.rit.edu/htbooks/nmr [38]. Useful sources for more general information about NMR and MRI physics include particularly: *Foundations of Medical Imaging* by Cho, Jones and Shing [18], *An Introduction to Magnetic Resonance* by Carrington and McLachlan [17] and *Magnetic Resonance Imaging* edited by Partain. Finally, a very cogent overview of the mathematics behind MRI and NMR can be found in papers by Hinshaw et al [35], Sebastiani et al [70] and Mezrich [57].

2.3.1 Basic Principles

Atomic nuclei which contain an odd number of protons and/or neutrons possess a net magnetic moment μ. These nuclei also possess angular velocity **J** related to the magnetic moment by Equation 2.8.

$$\mu = \gamma \mathbf{J}$$

Equation 2.8

γ is the gyromagnetic ratio, a fundamental nuclear constant that differs for every atomic element. In the absence of external magnetic fields, the magnetic moments are randomly oriented in space, and their vector sum is equal to zero. However, application of a magnetic field **B** results in a torque applied to the nucleus. Because the nucleus also has an angular momentum, **J**, the resulting motion is represented by:

$$\frac{d\mathbf{J}}{dt} = \mu \times \mathbf{B}$$

Equation 2.9

Equation 2.9 simply states that the rate of change of angular momentum is determined by the applied torque. Joining this equation to Equation 2.8, gives the following interesting expression:

$$\frac{d\mu}{dt} = \gamma(\mu \times \mathbf{B})$$

Equation 2.10

The magnetic moment changes in a direction perpendicular both to its direction and to the applied static magnetic field. Like a spinning top in a gravitational field, the magnetic moment begins to precess, as shown in Figure 2.5, around an axis parallel to the static field.

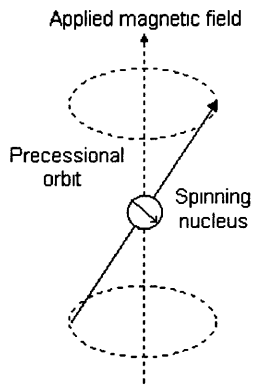

Figure 2.5: Spinning nucleus and associated magnetic moment. When a magnetic field is applied, the magnetic moment of the nucleus begins to precess about an axis parallel to the applied field.

The frequency of precession (ω in radians and f in Hertz), sometimes called the Larmor frequency, can be determined by solving Equation 2.10.

$$\omega = 2\pi f = \gamma |\mathbf{B}|$$

Equation 2.11

Quantum mechanics requires, in the presence of a static magnetic field $\mathbf{B_0}$, that a particle with a magnetic moment be in one of a finite number of energy levels. The actual number of energy levels is determined by the spin quantum number *I*, another

intrinsic characteristic of the nucleus in question. The energies associated with each level are also a function of the spin and the magnetic field.

$$E_I = \frac{\gamma h I |\mathbf{B_0}|}{2\pi} = \frac{h I \omega_0}{2\pi} = h I f_0$$

Equation 2.12

Note that the energy needed to move from one energy level to another is exactly the amount of energy stored in a photon at the Larmor frequency, $h f_0$.

The number of nuclei populating each energy level is determined by Boltzmann statistics (Equation 2.13). At room temperature, although the thermal excitation is sufficient to keep the population levels just about equal, there is a slightly larger number of nuclei, some constant proportion of the total population, at the lower energy levels.

$$\frac{N_H}{N_L} = e^{-\Delta E/kT}$$

Equation 2.13

$N_H \equiv$ number of nuclei at higher energy level
$N_L \equiv$ number of nuclei at lower energy level
$\Delta E \equiv$ difference in energy between energy levels
$T \equiv$ temperature
$k \equiv$ Boltzmann's constant

For a system with only two energy levels (^{1}H), Figure 2.6 depicts the arrangement of the nuclei both before and after a static magnetic field is applied. The excess magnetic moments in the lower energy level with its associated orientation of spins leads to the formation of a net magnetization **M** along the direction of the static magnetic field $\mathbf{B_0}$.

Magnetic resonance occurs when a radio frequency (RF) rotating magnetic field $\mathbf{B_1}$, applied at the Larmor frequency causes magnetic moments to flip between energy states. As Equation 2.12 showed, any photons at the Larmor frequency have the correct amount of energy to cause switching between levels. Since, at equilibrium as just shown,

there is an excess of spins in the lower energy state, absorption of energy takes place as spins are promoted to the higher energy levels. The RF pulse also serves to bring the phases of the individual magnetic moments into a coherent relationship. From a macroscopic perspective, this leads to the net magnetization vector **M** rotating away from its equilibrium state and precessing about the direction of $\mathbf{B_1}$ with a frequency ω_1 given by Equation 2.11. The direction of **M** is given in terms of the flip angle $\theta = \omega_1\tau$ where τ is the duration of the $\mathbf{B_1}$ pulse.

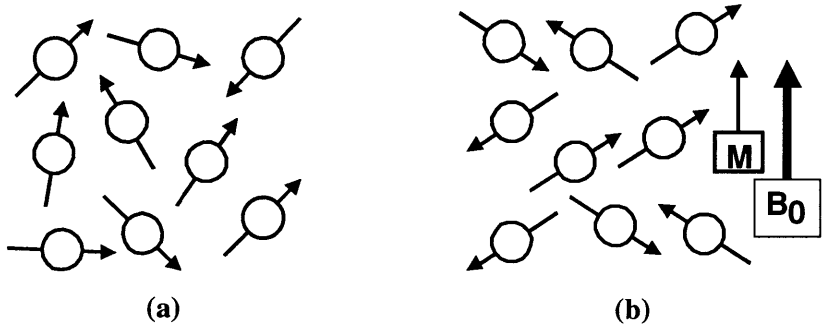

Figure 2.6: Nuclei before and after a static magnetic field B_0 is applied. (a) depicts the random arrangement of the magnetic moments before application of the field. (b) shows the B_0 field, and the resulting ordering of the magnetic moments into two groups, with one set pointing up (parallel spin) and the other pointing down (anti-parallel). The slight preponderance of those pointing up over those pointing down cause the generation of a cumulative magnetic moment M.

Figure 2.7 depicts the state of the net magnetization immediately after the $\mathbf{B_1}$ field is turned off. The deflected **M** continues to precess about the main $\mathbf{B_0}$ field as it slowly returns to equilibrium. The component of **M** in the transverse plane, $\mathbf{M_{xy}}$, acts to induce a current in a coil. The resulting exponentially decaying sinusoidal voltage is commonly referred to as free induction decay (FID). The FID constitutes the MR signal.

When more than one species of atom is involved, each type rotates at a different frequency, f_0, changing the shape of the FID by contributing a component at the new frequency.

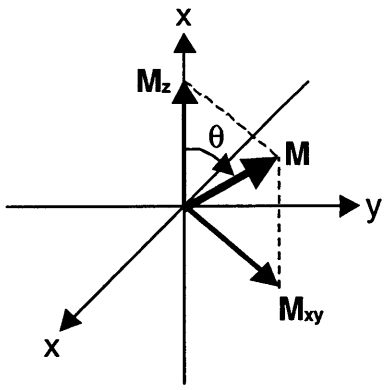

Figure 2.7: Depicted here is the state of net magnetization immediately after the excitation pulse, B_1, is turned off. M has been rotated away from the z-axis by an angle θ. Under the influence of the static magnetic field, it continues to precess about the z-axis which is collinear with the direction of B_0. This precession is reflected in the xy plane by the rotation of the transverse component of M, M_{xy}.

2.3.2 Signal Intensity

The magnitude of the FID corresponds directly to the magnitude of $\mathbf{M_{xy}}$. Immediately after the $\mathbf{B_1}$ pulse is switch off, the magnitude of $\mathbf{M_{xy}}$ is directly related, via the flip angle θ, to the magnitude of the net magnetization **M**.

$$| \mathbf{Mxy} | = | \mathbf{M} | \sin \theta$$

Equation 2.14

The magnitude of **M**, in turn, is directly related to the total number of nuclei. By measuring the initial magnitude of the FID, therefore, and given some standards against which to compare, it is possible to determine the total number of nuclei present. Further, according to Fourier theory, the area under the curve of the Fourier transform of a signal is equal to the initial magnitude of the FID. This means that a measure of the area under the Fourier transform of the FID can also serve as a measure of the number of nuclei present.

Measurements of nuclei-number via measurements of FID signal intensity can also be performed regardless of the number of different atomic elements that are present.

Since γ is different for every element, at a given static field strength $\mathbf{B_0}$, each element responds to a different excitation frequency. Only that portion of the total net magnetization due to the material of interest will respond to excitation at that frequency. Measurement of the FID, therefore, can theoretically be used to pick out the amounts of all magnetically active elements.

2.3.3 Relevant Time Constants

After excitation, the net magnetization vector **M** slowly returns toward its equilibrium state via a process called relaxation. Relaxation is characterized by two time constants T_1 and T_2. (Figure 2.9 and Figure 2.8.) These time constants depend on certain chemical and physical characteristics of the nuclei of interest, as well as on the properties of neighboring nuclei (which may consist of other elements). Measurements of differences in these time constants, therefore, can contribute useful information about elements other than those being directly excited by the RF radiation.

The spin-spin relaxation time, T_2, is the characteristic time associated with transverse magnetization relaxation. T_2 is quite important as it determines the amount of time available for stimulating and recording the FID. Equation 2.15, sketched in Figure 2.8, shows the relationship between T_2 and the transverse component ($\mathbf{M_{xy}}$)of the net magnetization **M**.

$$M_{XY} = M_d \, e^{-\frac{t}{T_2}}$$

Equation 2.15

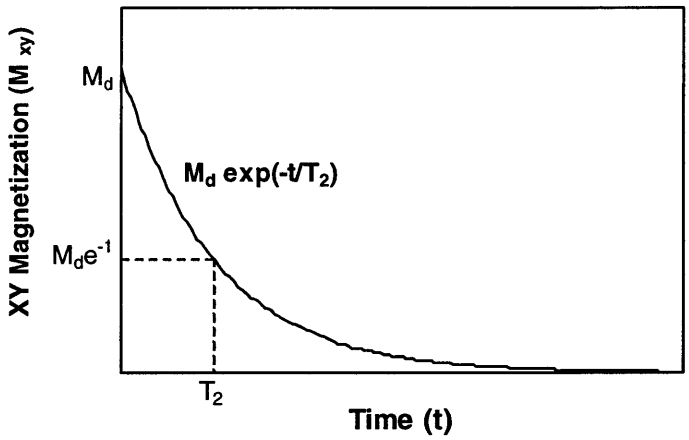

Figure 2.8: The spin-spin relaxation time describes the rate at which transverse magnetization, the detectable component of total magnetization, decays. M_d is the initial (detectable) transverse magnetization immediately after excitation.

The spin-lattice relaxation time, T_1, is the characteristic time associated with the regeneration of longitudinal magnetization, the z-component of **M**. Equation 2.16, sketched in Figure 2.9, shows the relationship between T_1, and the longitudinal magnetization.

$$M_z = M_0\left(1-e^{-\frac{t}{T_1}}\right)$$

Equation 2.16

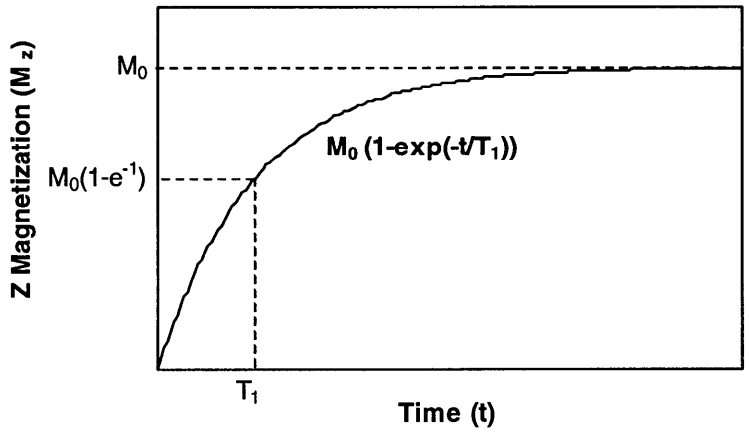

Figure 2.9: The spin-lattice relaxation time is associated with the renewal of the longitudinal component of the net magnetization vector. Here, M_0 represents the magnitude of the net magnetization M at equilibrium (before any excitation has taken place, or after the decay processes have been long completed).

Interestingly, because of the physical process that cause relaxation, T_2 is always less than T_1. This has the practical consequence of requiring a minimum recovery time between excitations since the transverse magnetization will have vanished below the noise level before longitudinal magnetization has completely recovered.

Measurements of T_1 are often made with what is known as an inversion recovery sequence. The flip angle θ is initially chosen to be 180° rather than the more usual 90°. Once **M** is flipped by 180°, it has no transverse component. Recovery of the signal, sketched in Figure 2.10, proceeds as described by Equation 2.17.

$$M_z = M_0\left(1-2e^{-\frac{t}{T_1}}\right)$$

Equation 2.17

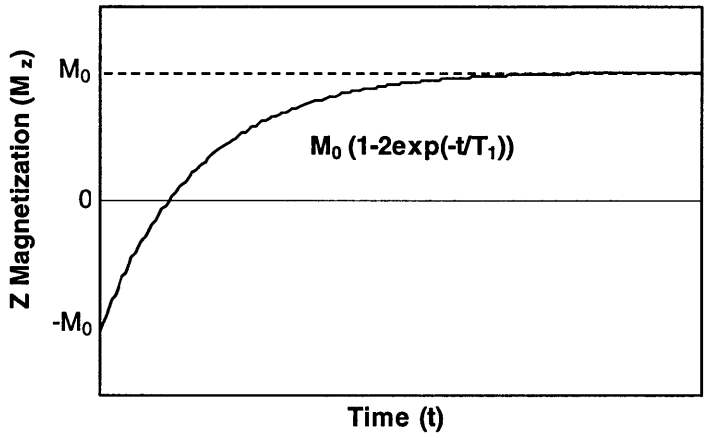

Figure 2.10: T_1 relaxation after a 180° pulse occurs as shown here. Once again, M_0 represents the magnitude of the net magnetization M at equilibrium (before any excitation has taken place, or after the decay processes have been long completed).

First applying a 180° pulse, waiting a time τ, and then applying a 90° pulse can identify specific points along this curve. The transverse magnetization after the second pulse will reflect the T_1 relaxation that occurred during time τ. After collecting several points by choosing different values of τ, a curve fit to an equation of the form of Equation 2.17 will give a value for T_1.

2.3.4 Contrast Agents

Contrast agents (so called because they can affect the contrast in MRI images) work by providing an extra source of magnetically active elements in solution so that relaxation can proceed faster. As the concentration of the contrast agent increases, the time constants decrease – relaxation happens faster. In general, the effect of contrast agent C on relaxation time constant T (the effect is applicable to both T_1 and T_2) is described by Equation 2.18 [84].

$$R[C] = \frac{1}{T_C} - \frac{1}{T_0}$$

Equation 2.18

where

$T_C \equiv$ value of the relaxation time constant in the presence of C.
$T_0 \equiv$ standard value of the relaxation time constant.
$R \equiv$ relaxivity of C.
$[C] \equiv$ concentration of contrast agent C.

The relaxivity, R, is a value that characterizes the efficiency with which the contrast agent increases water relaxation – decreases the time constant. It is important to note that since a particular contrast agent can affect T_1 and T_2 differently, the value of R can be different depending on the time constant in question. For a novel contrast agent, R can be calculated simply by measuring the effect, on the time constant of interest, of various concentrations of the contrast agent – one of those concentrations, of course, will be 0 M, in order to provide a value for T_0. Having calculated the value of R from solutions of known concentration, the concentration of C in unknown solutions can be determined by measuring one of the time constants.

2.4 Previous Work

The use of NMR/MRI to examine cartilage has been a topic in the literature for some time [4, 7, 29, 36, 47, 62, 39]. The non-invasive nature of MR as well as its marked ability to effectively image soft tissues, combined with the prevalence of cartilage diseases makes the combination quite appealing. Some of the work that has been done, however, is of particular importance for this work, as the experiments described below focus on particular aspects of this work.

2.4.1 Measurements with Sodium and Gadolinium

In 1992, Lesperance et al showed that NMR measurements of sodium ion concentration could be used to track tissue fixed charge density in cartilage via the Donnan model [47]. That paper also established that not only did sodium measurements track cartilage FCD, but the values so calculated were closely matched by values obtained by spectrophotometric assay methods. (Using bovine chondroitin sulfate as a standard led to a values of FCD that were 100 ± 7% of those calculated from sodium concentration measurements.) Bashir further explored the possibilities by looking at the implications of sodium T_1 and T_2 for imaging [4]. Unfortunately, not only is sodium MR complicated by extremely small T_2s, but the amount of sodium present in organic tissues is insufficient to provide a strong signal without repeating the scans many times for signal averaging purposes. Further, although sodium is ubiquitous in real physiological systems, *in vivo* studies using sodium MR are impractical. There is currently no means of quantifying the results of an *in vivo* sodium scan because of the interrelationship between the changing T_2s and the observed sodium signal. On the other hand, if sodium

concentrations could be measured quantitatively, that same ubiquity would make sodium measurement quite attractive despite its other problems.

Ionic contrast agent gadopentetate, Gd-DTPA^{-2} (Figure 2.11) [11], an FDA approved compound, is regularly used via injection in MRI studies. As such, there was information available on its use in other tissues [21] and its characteristics had been explored to some extent. [22].

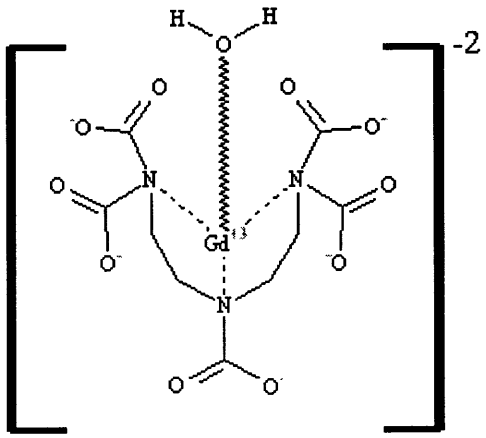

Figure 2.11: A chemical structural diagram of gadopentetate (Gd-DTPA^{-2}). The zigzag line in the picture represents a temporary weak bond with a water molecule in the neighborhood of the gadopentetate ion. By binding in this manner, the water molecule is forced to spend more time in the vicinity of the magnetically active Gd-DTPA^{-2}, which increases the relaxing effect.

In 1996, Bashir et al used measures of Gd-DTPA^{-2} in cartilage and Donnan theory to determine FCD [7]. They showed that, as with calculations using Na^+ and calculations using Gd-DTPA^{-2} resulted in values of FCD that correlated very nicely (r^2=0.94).

2.4.2 Effects of Particular Interest

Figure 2.12 is a copy of a graph published by Bashir et al. Note that the x and y axis both represent FCD. The only difference is that along the x-axis, FCD was calculated by measuring sodium concentration and applying the Donnan model. Along the Y-axis, on the other hand, FCD was calculated from measurements of gadopentetate

concentration. If the Donnan model adequately describes ion distribution, then the values calculated from the two measurements will be equal. However, this is not the case. In fact, the gadopentetate based values are related to the sodium based values by a line with a slope of $0.49 \approx \frac{1}{2}$. The goal of this work will be to examine one possible reason for this factor of two (or factor of one-half, depending on the viewpoint).

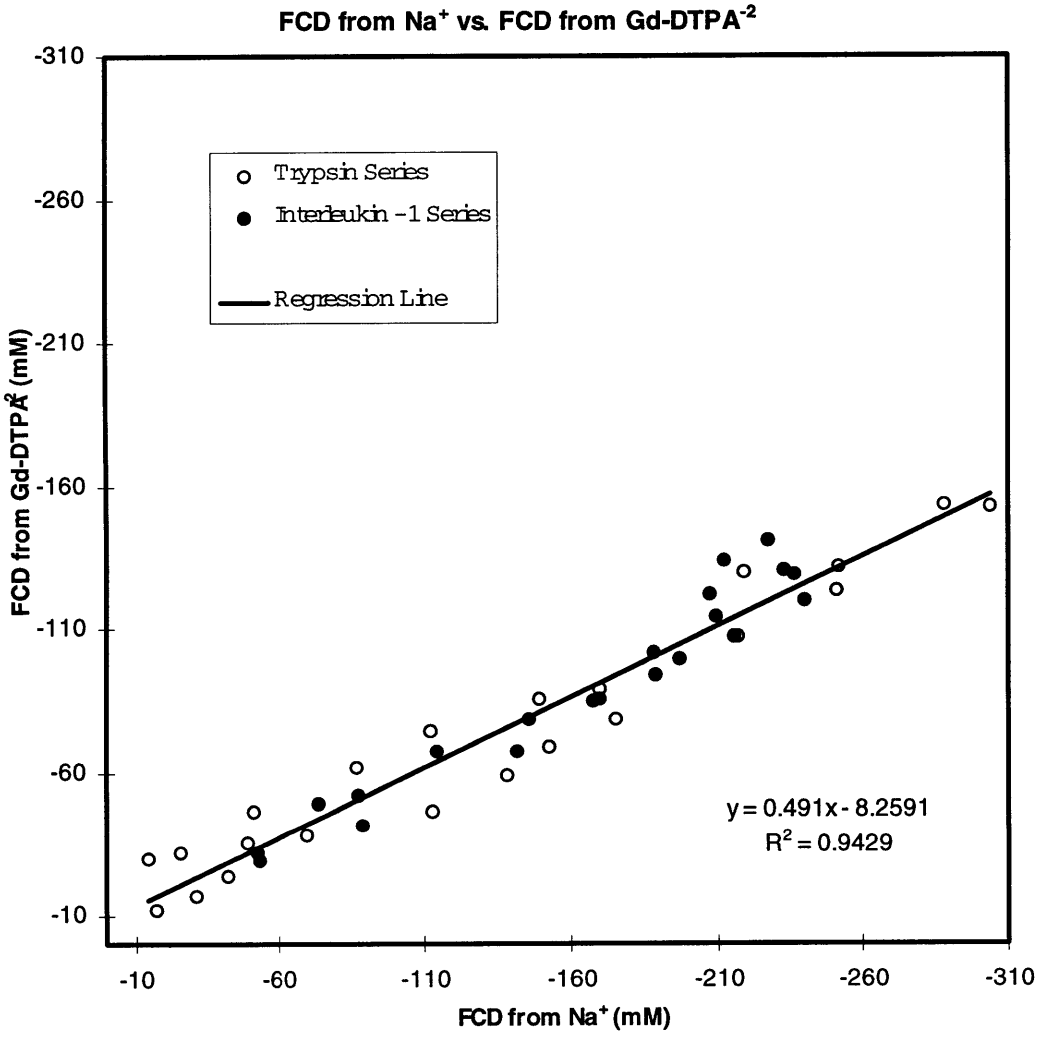

Figure 2.12: This data in this graph (copied with permission of the author) was published by Bashir et al in 1996 [7]. The x-axis is FCD as calculated from measurements of Na^+ concentration. The y-axis is FCD as calculated from measurements of Gd-DTPA^{-2} concentration. Both measurements were taken after equilibration in solution containing both sodium and gadopentetate. The slope of the regression fitted line shown is 0.49. The ideal Donnan model has no explanation for this factor of 2 difference in calculated values.

Chapter 3: Theoretical Analysis

The structure of cartilage provides one possible explanation for the factor of two ratio noticed in Bashir's experiments [7]. As Figure 2.1 suggests, the water content of cartilage is divided between two different regions: the intrafibrillar region, within the collagen fibrils, and the extrafibrillar region. In fact, roughly 30% of the tissue water can be found within the collagen fibers [51]. The important aspect of this division, however, is the fact that, due to the networked structure of the collagen bundles, the proteoglycans (and therefore the associated fixed charge) cannot enter the collagen fibers [55]. This means that the two water populations, intra- and extra- fibrillar, have different local fixed charge densities. Although the relationships outlined by Equation 2.1, Equation 2.2, and Equation 2.3 hold for each of the two regions, if compartmentalization is a factor, the relationships cannot be applied to the overall bulk of a cartilage sample.

The NMR methods developed by Lesperance et al [47] and Bashir et al [7], however, do not differentiate between the two water compartments. The values for sodium concentration and gadopentetate concentration calculated from NMR measurements reflect the volume averaged concentrations from each compartment.

$$\overline{C}_{M_i} = \overline{C}_{IF_i} v_{IF} + \overline{C}_{EF_i} v_{EF}$$

Equation 3.1

where

$\overline{C}_{M_i}$ ≡ volume averaged concentration of species *i* (measureable)

v_{IF} ≡ volume fraction of water in intrafibrillar space.

$\overline{C}_{IF_i}$ ≡ concentration of species *i* in intrafibrillar space.

v_{EF} ≡ volume fraction of water in extrafibrillar space.

$\overline{C}_{EF_i}$ ≡ concentration of species *i* in extrafibrillar space.

Since v_{IF} and v_{EF} are volume fractions, the following relation must hold true:

$$v_{IF} + v_{EF} = 1$$

Equation 3.2

Further, since the intrafibrillar space is charge free, at equilibrium, the concentrations of all ions within must be equal to the concentrations in the external solution. Only the concentrations of ions in the extrafibrillar space are affected by the fixed charge. In keeping with the notation introduced with Equation 2.1:

$$\therefore v_{IF} = 1 - v_{EF}$$
$$\overline{c}_{IF_i} = c_i$$
$$\overline{c}_{EF_i} = \overline{c}_i$$

Equation 3.1 can now be restated.

$$\overline{c}_{M_i} = c_i(1 - v_{EF}) + \overline{c}_i v_{EF}$$

Equation 3.3

3.1 Gd-DTPA^{-2} Based Calculations

Equation 3.3 provides the means to determine whether it is worthwhile to continue with this avenue of exploration. Spreadsheet based manipulations can provide an idea as to whether or not the partitioning of tissue water into two compartments has a significant effect on the ratio of FCD as calculated from measurements of Na^+ and Gd-DTPA^{-2}. Since measured concentrations are, in fact, the volume averaged concentrations of ions in the two compartments that compose cartilage, the fixed charge densities calculated using these measurements and the Donnan single compartment model must reflect the nature of the volume averaging. In fact, it is expected that FCD calculated from different ions will reflect volume averaging differently. Choosing a value to be the FCD as determined from Na^+, and working backward using Equation 2.1, Equation 2.2,

Equation 2.3 and Equation 3.3, a value for FCD as it would be calculated from Gd-DTPA^{-2} can be derived. (This derivation is outlined in Appendix A.) Figure 3.1 plots the ratio of the two FCDs as a function of volume fraction of the extrafibrillar compartment, showing the effect of the presence of two compartments on calculations of FCD using a single compartment Donnan model and measurements of Gd-DTPA^{-2} and Na^+ concentrations.

All the curves in the figure have a non-zero slope. The ratio of FCDs does depend on the volume of the extrafibrillar compartment in this simulation, which makes it possible that the ratio observed by Bashir et al [7] can be explained as due to the existence of two distinct water populations within cartilage. Further, healthy cartilage is composed of roughly 60mg/ml chondroitin sulfate and has a fixed charge density between –200 and –300mM. In this range, a ratio of 0.5 between FCD from Gd-DTPA^{-2} and Na^+ occurs for an extrafibrillar water content between 60 and 70%.

Table 3.1 contains data collected by Bashir. In the first four columns, the measured concentrations of sodium and gadopentetate in several samples under various bath conditions are marked down. Given these concentrations, FCD is calculated under the assumption that cartilage is a homogenous single compartment. As expected, the two values of FCD are unequal. Most of these data points appear in Figure 2.12 which shows the slope of the regression relationship between FCD calculated from Na^+ and FCD calculated from Gd-DTPA^{-2} as being equal to about 0.5. The last column of Table 3.1 contains values for the volume of extrafibrillar water needed in order for a two compartment model to correctly explain the measured values. As shown in Appendix B, given the assumptions behind Equation 3.3, it is possible to derive the extrafibrillar

compartment volume fraction from measured tissue ion concentrations and known bath concentrations. Only one such volume will permit Donnan equilibrium to hold.

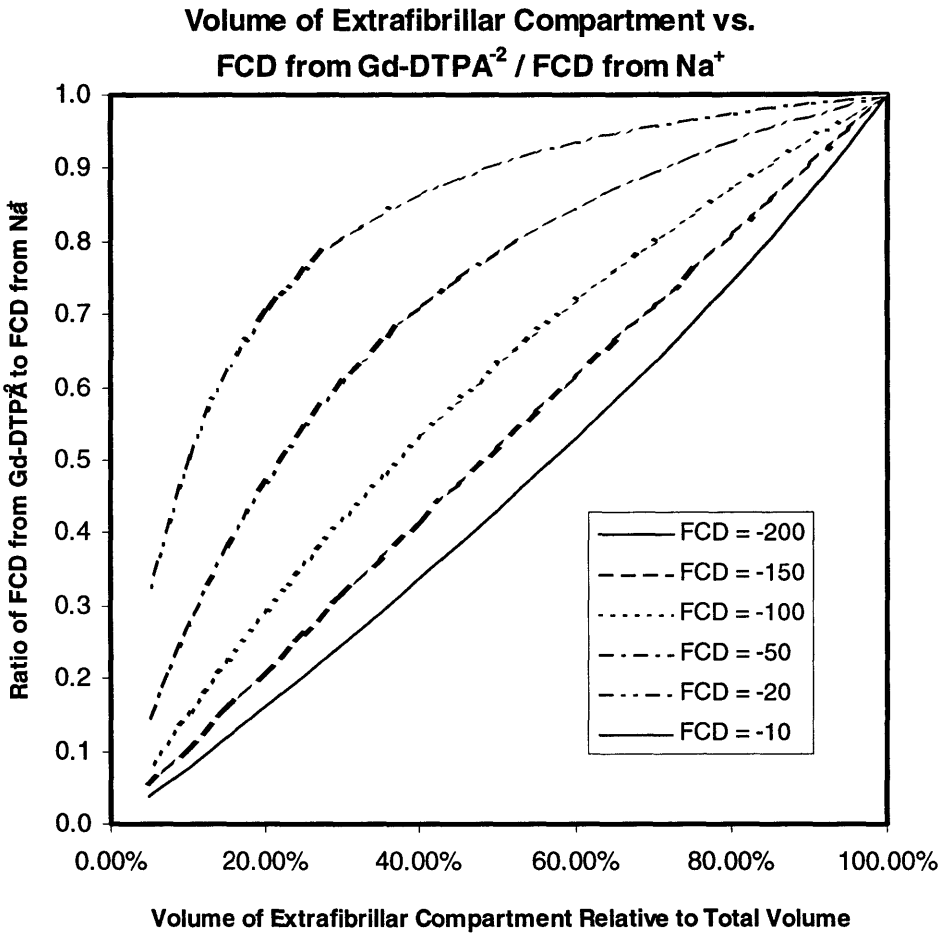

Figure 3.1: Values for FCD as calculated from sodium are chosen. Each value is then used to determine FCD as it would be calculated from gadopentetate, and the ratio of the two numbers is taken. This value is plotted versus the volume fraction of the total cartilage water content that is found within the extrafibrillar space. It was also assumed, plotting these curves, that bath concentrations of Na^+ and Gd-$DTPA^{-2}$ were 150mM and 1mM respectively. Note that none of these curves are horizontal lines, showing that this ratio is, indeed, dependent on the volume of the extrafibrillar compartment. Further, all curves meet when 100% of the volume is extrafibrillar. At that point, an ideal single compartment exists. Although not shown here, the curve generated for an FCD of –300mM shows a ratio of 0.51 at 70% extrafibrillar water.

Sample Name	$[Na^+]$ in Bath	$[Gd\text{-}DTPA^{-2}]$ in Bath	$[Na^+]$ in Tissue	$[Gd\text{-}DTPA^{-2}]$ in Tissue	FCD from $[Na^+]$	FCD from $[Gd\text{-}DTPA^{-2}]$	Extrafibrillar Compartment Volume Fraction
C1	150.0	1.000	271.1	0.550	-188.1	-91.0	0.535
C2	150.0	1.000	298.4	0.470	-223.0	-116.0	0.623
C3	150.0	1.000	285.5	0.480	-206.7	-112.6	0.624
C4	150.0	1.000	331.0	0.420	-263.0	-134.2	0.664
C5	150.0	1.000	328.1	0.420	-259.6	-134.2	0.666
C6	150.0	1.000	326.8	0.420	-257.9	-134.2	0.667
C7	150.0	1.000	382.7	0.330	-323.9	-174.9	0.750
C8	150.0	1.000	327.5	0.440	-258.8	-126.6	0.638
E1	150.4	0.500	325.0	0.168	-255.4	-172.4	0.796
E2	150.4	0.500	345.0	0.178	-279.4	-162.0	0.742
E3	150.4	0.500	393.3	0.122	-335.8	-230.5	0.860
E4	150.4	0.500	417.8	0.120	-363.7	-233.6	0.849
E5	150.4	0.500	449.3	0.125	-399.0	-225.6	0.820
E1	150.4	1.000	323.4	0.348	-253.5	-166.4	0.780
E2	150.4	1.000	340.3	0.312	-273.8	-185.4	0.813
E3	150.4	1.000	390.2	0.271	-332.2	-210.8	0.825
E4	150.4	1.000	418.9	0.269	-364.9	-212.0	0.810
E5	150.4	1.000	424.8	0.241	-371.6	-232.6	0.843
E1	150.4	2.000	328.7	0.825	-259.9	-137.6	0.677
E2	150.4	2.000	345.7	0.733	-280.2	-157.4	0.727
E3	150.4	2.000	384.4	0.612	-325.5	-188.7	0.781
E4	150.4	2.000	405.3	0.558	-349.4	-205.4	0.805
E5	150.4	2.000	431.0	0.572	-378.5	-200.7	0.782
					Average of Extrafibrillar Compartment Volume Fraction:		0.7425
					Std. Dev. of Extrafibrillar Compartment Volume Fraction:		0.0888

Table 3.1: The data in the first four columns of this table is a collation of data gathered by Bashir using bovine cartilage samples. Note that all concentrations are in units of mM. Given ion concentrations in equilibrating solution as well as measured ion concentrations in the tissue, FCDs are calculated treating the tissue as a single homogenous compartment. As Bashir et al demonstrated [7], FCDs calculated in this manner from measurements of [Na+] and [Gd_DTPA-2] are unequal. The last column contains the relative volume fraction of the extrafibrillar compartment required to force sodium and gadopentetate measurements to give the same value for FCD in the extrafibrillar space. The average and standard deviation of these values are presented as well. These data seem to suggest that roughly 70% of the sample water was in the extrafibrillar space.

As can be seen, most of the samples listed here would satisfy Donnan and have a volume averaged tissue concentration equal to the measurements if about 70% of tissue water was extrafibrillar. In fact, as the calculations at the bottom of the table show, the average required volume was 74%, with a standard deviation of 9%. The 70% value

derived here also agrees with values reported by Maroudas for valuations of water content of the extrafibrillar space. [51].

3.2 Cl^- Based Calculations

Having shown that the one to two ratio observed can theoretically be described by utilizing a two compartment model of cartilage, it was decided to determine if the same effect would be observed for calculations of FCD using measurements of chlorine ion concentration. The first step, once again, was to work backward from a chosen value of FCD as calculated from Na^+.

Using Equation 2.1, Equation 2.2, Equation 2.3 and Equation 3.3, the FCD as it would be calculated from Cl^- measurements can be found (Appendix A). Figure 3.2 plots the ratio of these two FCDs against the relative volume of the extrafibrillar compartment, showing the effect of the presence of two compartments on calculations of FCD using a single compartment Donnan model and measurements of Cl^- and Na^+ concentrations.

In order to examine this theoretical finding, the literature provides a source of experimental data. In 1972, Evans and Maroudas published a paper [52] describing research in which they made use of radiotracer methods to measure the concentrations of Na^+ and Cl^- ions in cartilage after it was allowed to equilibrate in solutions of known concentrations. Along with the relevant analysis, this paper included much of the raw data that was collected. Table 3.2 tabulate part of this data in the first 5 columns. (The first two columns simply identify the different samples.) For space reasons, several samples that were not used for the purposes of this paper were not included in the table. These samples were ignored for one of two reasons. In some cases, the data published contained what appeared to be typographical errors, as the values appeared to be a factor

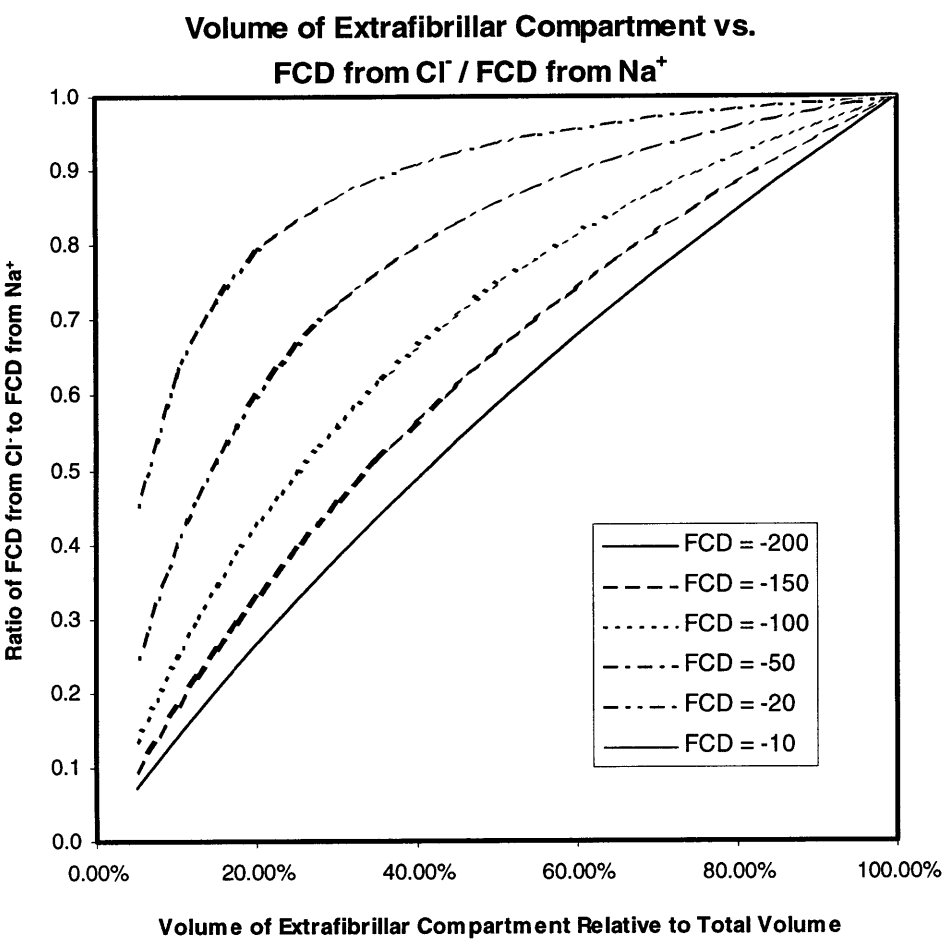

Figure 3.2: Values for FCD as calculated from sodium are chosen. Each value is then used to determine FCD as it would be calculated from chlorine, and the ratio of the two numbers is taken. This value is plotted versus the volume fraction of the total cartilage water content that is found within the extrafibrillar space. It was also assumed, plotting these curves, that bath concentrations of Na^+ and Cl^- were 150mM. Note that none of these curves are horizontal lines, showing that this ratio is, indeed, dependent on the volume of the extrafibrillar compartment. Further, all curves meet when 100% of the volume is extrafibrillar. At that point, an ideal single compartment exists. Qualitatively, these curves very much resemble those shown in Figure 3.1 for Gd-DTPA^{-2}

of 10 greater or less than that of similar samples. Also ignored were samples equilibrated at bath concentrations of NaCl lower than 100 mM. Maroudas and Evans acknowledged in their paper that at low bath concentrations, the activity coefficients of the ions in cartilage were significantly different from the activity coefficients in the bath.

Subject Age	Sample #	[NaCl] in Bath	$[Na^+]$ in Tissue	$[Cl^-]$ in Tissue	FCD from $[Na^+]$	FCD from $[Cl^-]$	Extrafibrillar Compartment Volume Fraction
33	1	150.0	222.0	97.1	-120.6	-134.6	1.329
	2	150.0	248.0	99.0	-157.3	-128.3	0.709
	3	150.0	279.0	81.0	-198.4	-196.8	0.989
	4	150.0	319.0	73.1	-248.5	-234.7	0.941
	5	150.0	306.0	66.5	-232.5	-271.8	1.198
45	1	150.0	205.0	106.0	-95.2	-106.3	1.467
	2	150.0	256.0	91.0	-168.1	-156.3	0.887
	3	150.0	288.0	82.6	-209.9	-189.8	0.878
	4	150.0	306.0	69.4	-232.5	-254.8	1.112
	5	150.0	320.0	64.6	-249.7	-283.7	1.144
67	1	150.0	174.0	132.0	-44.7	-38.5	0.480
	2	150.0	198.0	105.0	-84.4	-109.3	4.800
51	1	140.0	224.0	102.0	-136.5	-90.2	0.496
	2	140.0	267.0	81.5	-193.6	-159.0	0.775
	3	140.0	315.0	73.5	-252.8	-193.2	0.766
	4	140.0	260.0	59.5	-184.6	-269.9	1.747
40	1	138.0	174.0	128.0	-64.6	-20.8	0.100
	2	138.0	183.0	107.0	-78.9	-71.0	0.722
	3	138.0	204.0	98.9	-110.6	-93.7	0.695
	4	138.0	228.0	83.4	-144.5	-144.9	1.006
51	1	100.0	145.0	94.4	-76.0	-11.5	0.064
	2	100.0	172.0	69.0	-113.9	-75.9	0.544
	3	100.0	165.0	56.9	-104.4	-118.8	1.279
Average of Extrafibrillar Compartment Volume Fraction:							1.049
Std. Dev. of Extrafibrillar Compartment Volume Fraction:							0.910

Table 3.2: The data in the first five columns of this table is copied from data published by Evans and Maroudas [52]. Note that all concentrations are in units of mM. Given ion concentrations in equilibrating solution as well as measured ion concentrations in the tissue, FCDs are calculated treating the tissue as a single homogenous compartment. Interestingly, the calculated FCDs are sometimes fairly close to each other, and sometimes quite far apart. The last column contains the relative volume fraction of the extrafibrillar compartment required to force sodium and chlorine measurements to give the same value for FCD in the extrafibrillar space. The average and standard deviation of these values are presented as well. The average value calculated here is actually greater than 1 (this is biased heavily by a single sample – sample 2 from subject age 67) which is impossible. Considering that quite a few of the individual samples also require an extrafibrillar volume fraction greater than one in order to set FCD from Na^+ equal to FCD from Cl^-, however, it seems clear that either the two compartment model does not well suit this data, or these data are inaccurate..

Since the remainder of the data presented in this work was obtained under conditions of Donnan equilibrium, it seemed reasonable to ignore data recorded under different conditions. Further, low bath concentrations of NaCl leads to even lower tissue concentrations of Cl^- in the tissue due to the nature of the Donnan partitioning. At such low concentrations, small errors in measurement can comprise large errors relative to the magnitude of the overall measurement.

In columns four and five, the measured concentrations of sodium and chlorine in several samples under various bath conditions are marked down. Given these concentrations, FCD is calculated under the assumption that cartilage is a homogenous single compartment. In this case, the two values of FCD are sometime quite close and sometimes quite far apart. Figure 3.3 plots FCD as calculated from sodium vs. FCD as calculated from chlorine in Table 3.2. As the graph shows, the slope of the regression relationship between the two is quite close to one, which, given Figure 3.2, is unexpected. The last column of Table 3.2 contains values for the volume of extrafibrillar water (calculated, once again, using the relations outline in Appendix B) necessary for a two-compartment model to correctly describe the measured values. Observe that many of the samples require a volume fraction greater than one in order to satisfy the requirement of equal FCDs from either measurement. Given the definition of the volume fraction (proportion of total sample water in the extrafibrillar space), it is impossible for the value to be greater than one.

Neither the data in Table 3.2, nor the plot in Figure 3.3 support a two-compartment model for cartilage. On the other hand, given the large variance in

extrafibrillar volume fraction, neither do they completely exclude the possibility. Further exploration is warranted.

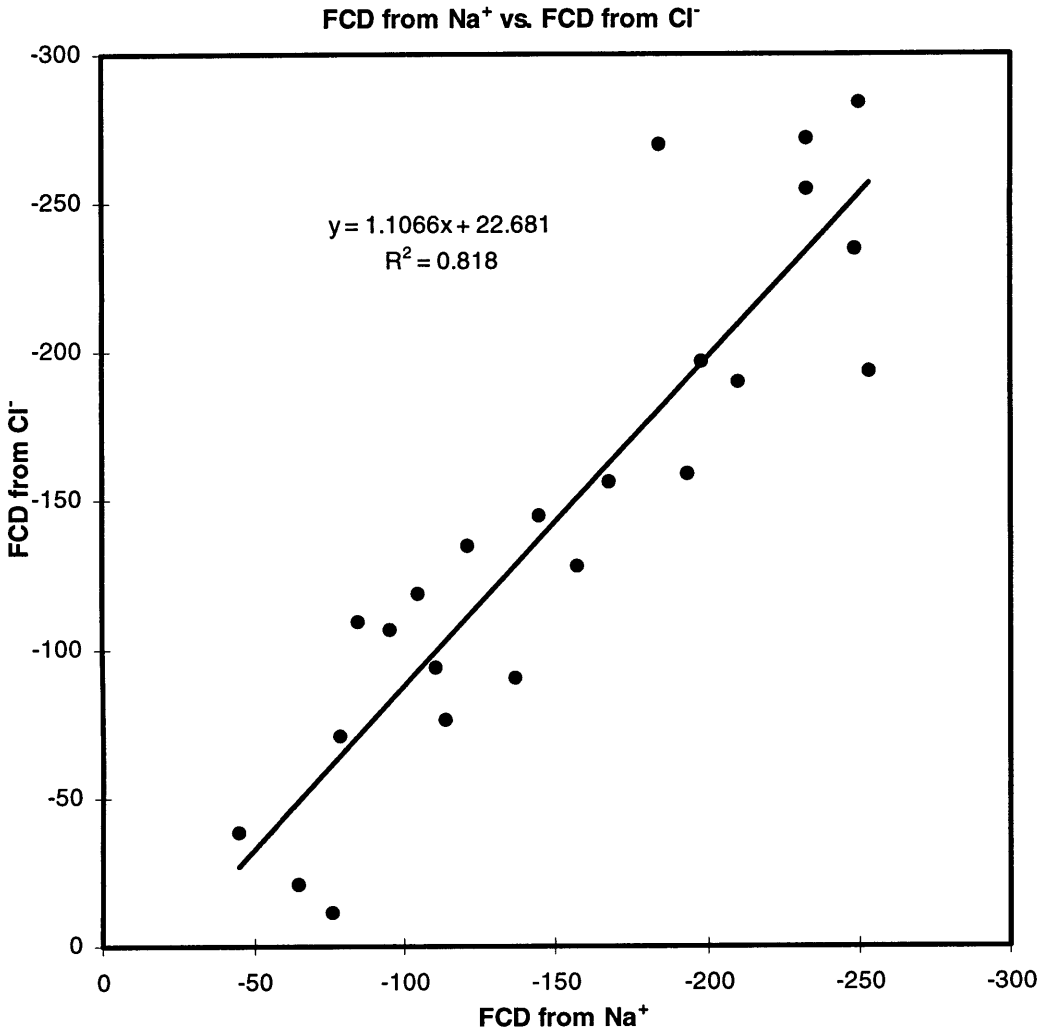

Figure 3.3: A plot of FCDs as calculated from measurements of sodium concentration vs. FCDs as calculated from chlorine concentration. The slope of the regression line is 1.11, fairly close to the value expected if the system was well described as a single ideal Donnan compartment.

3.3 Na^+ Measurements

One last aspect of the two-compartment model that was explored on a theoretical basis was the effect of the two compartments on the validity of FCD measurements using Na^+ ion concentrations. Since it has been validated by Lesperance et al that such

measurements do actually result in reasonable values of FCD in cartilage [47], this last consideration is quite important.

FCD calculated using the Donnan single compartment model and a volume averaged measurement of sodium ion concentration is compared to volume averaged FCD (Figure 3.4). Data was generated by once again working backwards from a chosen value of FCD as calculated from Na^+ measurements. A route can be traced from sodium

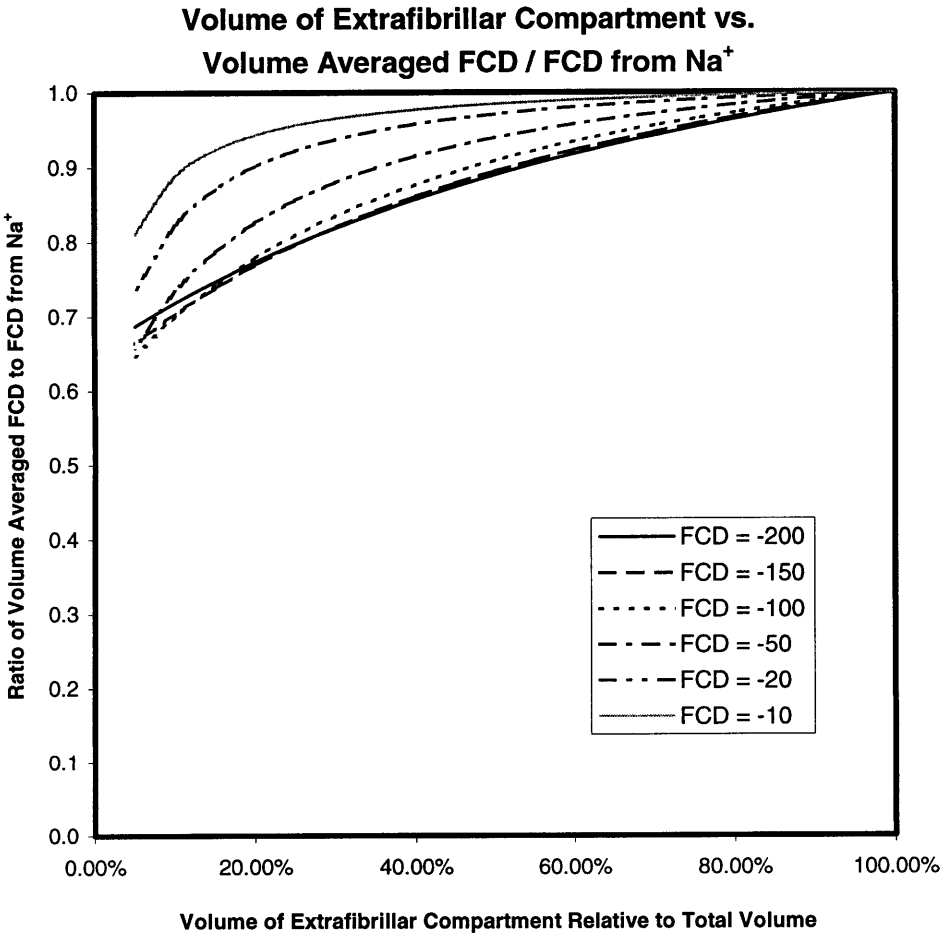

Figure 3.4: Values for FCD as calculated from sodium are chosen. Each value is then used to determine actual FCD in the extrafibrillar compartment. From this value, a volume averaged FCD is calculated, and its ratio to the originally chosen value is taken. This value is plotted versus the volume fraction of the total cartilage water content that is found within the extrafibrillar space. It was assumed, plotting these curves, that bath concentrations of Na^+ 150mM. The largest differences between volume averaged FCD and FCD from sodium measurements occurs in the low FCD region.

based FCD to average sodium concentration to sodium concentration in extrafibrillar space to FCD in extrafibrillar space. Since there is no fixed charge in the intrafibrillar space, determining the volume averaged FCD is a matter of dividing by total volume. The ratio obtained by comparing this derived value to the number with which the process started shows the effect of having two compartments when computing FCD from a single compartment model and measurements of Na^+ concentration.

The key point here is that, compared to Figure 3.1 and Figure 3.2, the curves curves in Figure 3.4 are almost flat. Clearly, compartmental volume fractions do have an effect on the calculated value of FCD, but the error is less that 10% at all fixed charge densities as long as the extrafibrillar volume fraction is greater than 50%.

3.4 Hypothesis

Given the theoretical analysis above, it seemed possible that the factor of two observed by Bashir et al [7] could, at least in part, be due to the presence of two compartments, the intrafibrillar and the extrafibrillar, within cartilage. If this was the correct reason, then a material consisting of only a single compartment should not show the factor of two. More clearly, the hypothesis being tested in this work is: *A true single compartment system should show little difference between FCD as calculated from sodium ion concentration and FCD as calculated from gadopentetate concentration using a single compartment Donnan model.*

Chapter 4: Methods

4.1 Cartilage Preparation w/Trypsin

Initially, an attempt was made to obtain a single compartment that was intrafibrillar in nature (containing no fixed charge). In order to do this, cartilage explants from calf ulnae were treated with trypsin to remove the proteoglycans. The remaining collagen rich material was subjected to NMR measurements.

4.1.1 Epiphyseal Cartilage Explant

Bovine epiphyseal cartilage was obtained from distal ulnae of newborn calves. Intact joints were obtained immediately after slaughter. The distal ulna of each joint was exposed by cutting away surrounding muscle and tissue. The ulnar periosteum was removed with care, the ulna separated from the radius, and then broken at the metaphyseal/epiphyseal cartilage interface. The epiphyseal cartilage with attached bony epiphysis was placed in Hank's solution to prevent dehydration.

Each epiphysis was then fixed in a sledge microtome and slices 1mm thick were sectioned. The last slice on each end was discarded to ensure all the slices used were of uniform thickness and contained no bone fragments. From each slice, 7mm diameter cylindrical disks were cored using a dermal punch.

Each disk was then blotted dry and placed in a centrifuge tube. All tubes were placed in the freezer until needed.

4.1.2 Trypsin Degradation

Trypsin degrades cartilage, causing loss of noncollagenous proteins and proteoglycans from the extracellular matrix leaving behind primarily pure collagen.

Total cartilage water content is affected because the loss of proteoglycan causes a decrease in swelling.

After one set of NMR measurements, cartilage samples were removed from the freezer and bathed overnight in 2 ml saline containing 2.5 mg/ml trypsin. Cartilage was then removed from the trypsin and bathed in 2 ml fetal calf serum for several hours to halt trypsin activity. The now visibly 'gooey' samples were put in centrifuge tubes and returned to the freezer.

4.1.3 Just Prior to NMR

All cartilage samples were removed from the freezer and equilibrated in plain Hank's solution or in Hank's solution with an addition 1mM Gd-DTPA^{-2} for at least 3 hours before any NMR measurements were made.

4.2 Single Compartment Model Preparation

Attempts were also made to emulate the extrafibrillar region of cartilage. Suspensions of chondroitin sulfate were placed in dialysis bags and immersed in Hank's solution with 1mM Gd-DTPA^{-2}. After equilibration, samples of the solutions with the dialysis tubes were subjected to NMR measurements.

4.2.1 Charge Rich Solution

It has been shown that cartilage proteoglycan is approximately 60mg/ml water. In order to emulate cartilage as closely as possible, a solution of 100mg/ml shark chondroitin sulfate C (C4348 form shark, Sigma Chemical) was made up by measuring 1 g into 10 ml Hank's solution. 4 ml of the 100mg/ml solution were transferred to a separate container, and the remaining 6ml put in the freezer. Using the 4ml put aside,

serial dilutions were made (Figure 4.1) by transferring 2ml of each solution into another container and mixing in 2ml of additional Hank's solution. Concentrations of 50mg/ml, 25mg/ml, 12.5 mg/ml, and 6.25mg/ml were made by serial dilution. Adding only 2ml Hank's solution to a sixth container made a concentration of 0mg/ml. The frozen 6ml of 100ml/mg solution was used for similar experiments later in time.

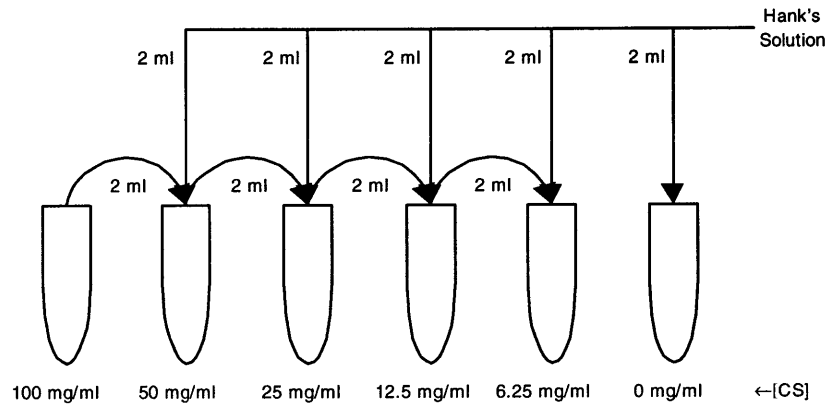

Figure 4.1: Serial dilutions for making chondroitin sulfate solutions of different concentrations. The first 100mg/ml solution was mixed up separately.

4.2.2 Dialysis Bag Apparatus

Once the solutions of chondroitin sulfate were made, a mechanism of suspending it in equilibration solution was necessary. To that end, cellulose dialysis membrane (Spectra Por MWCO 1000) was used. A molecular weight cut-off (MWCO) of 1000 means that the membrane is permeable primarily to compounds under 1000 g/mol. Larger molecules can permeate, but not to any great extent. As Figure 2.4 shows, the molecular weight of the chondroitin sulfate disaccharide is only 459.37 g/mol. The purchased chemical is obtained in a polymerized form, and is, therefore, at least twice as massive and unable to diffuse through the dialysis tube. Although there is the possibility of some loss of material due to the presence of some monomers, most of the chondroitin sulfate will be retained.

Instructions sent from Spectra Por regarding membrane preparations were followed exactly. Six strips approximately 7 inches long were cut. The strips were rinsed with distilled water for some time in order to remove excess sodium azide (toxic storage medium). A marble was placed about 1 inch from the base of each strip, and that inch was folded over to trap the marble in a little loop of tubing. A dialysis tube closure (Spectra Por Closures) was used to seal the loop, holding the marble in place by keeping the loop tight. Note that if colored marbles are used, recording the different colors provides a means for keeping track of which solution is placed in which piece of tubing.

1.6ml of one of the previously prepared (Figure 4.1) chondroitin sulfate samples was placed in one dialysis tubing apparatus with a Pipetman micropipette. Carefully holding the tube at the unsealed end, any air bubbles were cleared out, and another closure applied to seal the liquid into the central region. It is important to ensure that the second closure closes over a region containing some of the sample fluid. This ensures that some of the fluid is forced back into the central region , increasing the hydrostatic pressure within the tube and assuring that osmotic effects will not cause too much dilution of the contents of the tube.

Any excess dialysis tubing extending beyond the second closure was removed, and the tubing/closure/marble apparatus was placed into a glass beaker full of equilibration solution (to be described). The process just described was then repeated for the remaining five samples. Finally, a magnetic stirring bar was added to the beaker, the beaker top (Figure 4.2) was sealed with parafilm (to prevent water loss from evaporation) and the beaker was placed on a stirring pad in the refrigerator. It was left to equilibrate for one week.

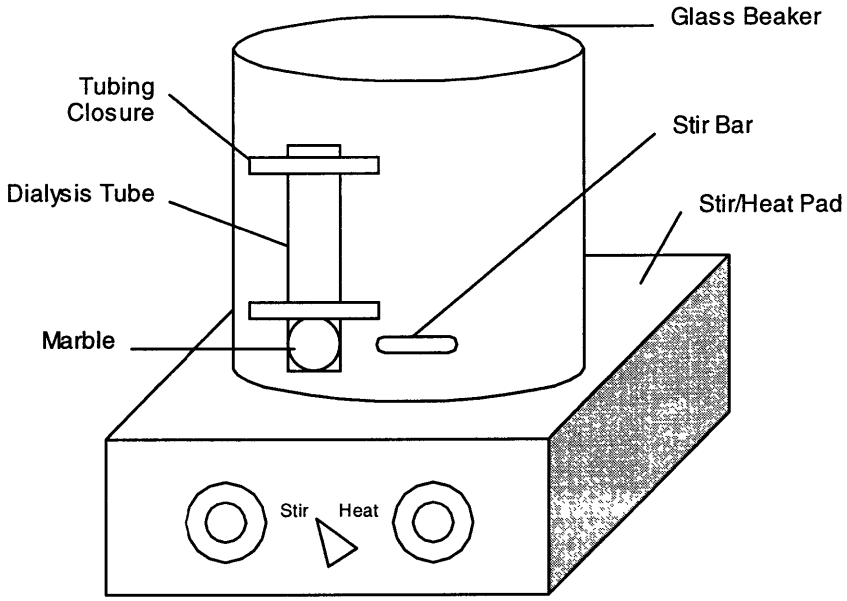

Figure 4.2: Dialysis bag apparatus. Glass beaker, here depicted with only one sample, can hold all six samples simultaneously. Each tubing apparatus floats marble side down in the equilibration solution. The tubing closures are lighter than water. Not only do the marbles help to weigh down each bag, but they also help to orient each one vertically.

At the end of the week, the beaker was removed from the refrigerator and individual bag concentrations identified (by marble color). Remove beaker from refrigerator and identify individual bag concentrations. One sample tube was picked and help marble-side up in order to let excess equilibration solution drip away. The closure near the marble was carefully removed, with care taken to maintain a safe grip on the dialysis bag. After unfolding the tubing and removing the marble, the tubing was visually inspected to determine the height of liquid within. Scissors were used to snip the tubing halfway across about 1/8 inch above the level of the liquid.

Through this gap was inserted the thin nose of a glass pipette attached to an evacuated rubber bulb. As much as possible of the liquid within the tube was removed to a labeled centrifuge tube. This process was repeated for the remaining five samples as

well. The centrifuge tubes were put into the freezer until the time came for NMR measurements.

4.2.3 Equilibration Solution

The equilibration solution used in these experiments, both with trypsin-treated cartilage and with the dialysis-tubing apparatus, was quite simple to make. For measurements in the absence of contrast agent, Hank's solution (GibcoBRL), which is 148 mM in Na^+ was used. For measurements with contrast agent, a 1 mM contrast agent solution was produced by mixing 499 ml Hank's solution with 1 ml contrast agent. Two sets of experiments were done. In one, a charged ionic contrast agent, Magnevist brand gadopentetate dimeglumine (Gd-DTPA^{-2}) was used. In another experiment, a non-ionic contrast agent, ProHance – brand name – took part.

4.2.4 Just Prior to NMR

Unlike cartilage samples, which need to be equilibrated just before scanning, the samples of chondroitin-sulfate-rich fluid need only be thawed. 50μL aliquots of each sample were put into MR sample vials (small glass tubes with a diameter of a few millimeters) for imaging.

4.3 NMR Measurements

The various NMR parameters need not be outlined in detail here. The procedures followed were almost exactly as outlined by Bashir et al. The reader is referred to their paper [7] for details on the NMR methods beyond the few items and exceptions noted here.

All measurements were on an 8.45 Tesla Bruker spectrometer (Bruker Instruments). Cartilage samples were first blotted dry and weighed. All samples were then placed in a dual 10/15mm ($^{23}Na/^{1}H$) broadband probe for measurements.

T_1 was measured with an inversion recovery sequence. Contrast agent relaxivity was calculated, using Equation 2.18, from only two measurements, in the absence and in the presence of a known concentration of contrast agent in Hank's solution. It has already been shown that relaxivity of gadopentetate in normal and degraded cartilage is equal to that in saline [22], so use of relaxivity measured in Hank's is justified for calculations in cartilage and in chondroitin sulfate solutions. Although the same has not been shown for ProHance, such was assumed to be true. T_1 measurements in samples were then also put through Equation 2.18 with the calculated relaxivity in order to determine contrast agent concentration ([Gd-DTPA^{-2}] and [ProHance]). Since the chondroitin sulfate solutions at their final concentrations were available for NMR only after equilibration, T_1 in the absence of contrast agent was not measurable. The value obtained for T_1 in Hank's without contrast agent was used instead. This procedure was validated by making T_1 measurements with varying amounts of chondroitin sulfate and no contrast agent to determine the relaxation effect of the chondroitin sulfate.

Sodium spectra were obtained by a one pulse sequence with 2000 averages. Sodium content was determined from sodium spectra by calibration to a set of standards – solutions of known sodium concentrations.

Proton spectra were also obtained by a one pulse sequence. Water content was similarly calculated from proton spectra by calibration to a set of standards. (Although there are protons within all the samples that are not part of water, since an overwhelming

majority of the protons are from water, the contribution of those other protons is assumed to be inconsequential.) Note that, for the cartilage trypsinization experiments, water content of cartilage prior to trypsinization was calculated as 70% of the wet weight, assuming that about 70% of cartilage mass was composed of water which has a density of 1g/ml.

Given water content from proton spectra and sodium content from sodium spectra, sodium concentrations were easily calculated.

FCDs were calculated with Equation 2.7 using the concentrations evaluated above where possible. Note that measurements of ProHance did not give FCD, as a non-ionic agent theoretically does not distribute in a manner dependent on FCD.

4.4 Spectrophotometric Assay

After NMR measurements were completed, all dialyzed samples were analyzed for CS content by using the dimethylmethylene blue (DMB) assay [24]. Absorbances were obtained at 525nm with a Lambda 3B spectrophotometer (Perkin-Elmer). Conversion to concentrations was done by comparison to standards generated from the same chondroitin sulfate used for the original samples. In previous work, it had been observed that choice of standard could affect the outcome of the assay [47]. In this case, since both samples and standards come from the same source, the concentrations obtained by these comparisons to standards should reflect the actual composition of the samples. Since the DMB standard concentrations range from 0 to 1000 μg/ml, it was usually necessary to dilute samples 1:10 or 1:100 since sample concentrations were in the mg/ml range. (Of course, no dilution was needed for the 0 mg/ml sample.)

Calculation of FCD from the concentrations found through the DMB assay was based on two assumptions. First, the molecular mass of CS was assumed to be 503.34g/mol as calculated from the chemical structure in Figure 2.4 and taking into account that the purchased chemical was a sodium salt (two sodium atoms per disaccharide). Second the charge on each monomer was assumed to be –2. FCD was then calculated by dividing the concentration (mg/ml) by the molar mass (g/mol), multiplying by –2 (-2 units charge per monomer) and multiplying by 1000 to find FCD in mM rather than in M units.

The presence of gadopentetate in samples being analyzed with the DMB assay was a concern. Chemical interaction between the anionic gadopentetate and the cationic components of DMB could have affected the assay result. An experiment was done to test whether a reaction occurred. 4ml of 1075µg/ml CS were made by weighing 4300µg of CS into 4ml Hank's solution. 1ml of 50mM Gd-DTPA^{-2} was made by mixing 0.9ml Hank's solution with 0.1ml 500mM Gd-DTPA^{-2}. Serial dilutions (Figure 4.3) were made as shown. 500 µl of each dilution were mixed with 500 µl of the prepared 1075µg/ml CS solution.

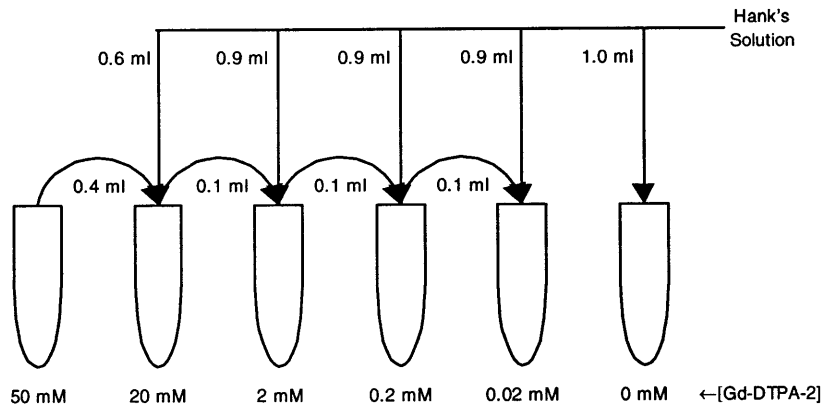

Figure 4.3: Serial dilutions for making Gd-DTPA^{-2} solutions of different concentrations. The first 50mM solution was mixed up separately.

The final solutions all contained 537.5μg/ml of CS and were between 25 mM and 0.01 mM in Gd-DTPA^{-2}. These solutions were then assayed with the DMB assay, and CS concentration calculated based on those measurements. The standards for the DMB assay were generated using 500 μl of the same 1075μg/ml CS solution.

Chapter 5: Results & Discussion

This section will present results mainly from three different experiments, with supporting experimental results occasionally provided.

5.1 Cartilage Measurement

The first attempt at generating a single compartment – this one with no fixed charge - was made by degrading cartilage with trypsin. Table 5.1 tabulates the FCDs calculated from ion concentration data collected before and after trypsin degradation.

Calculated FCDs (M)						
	Before Trypsin			After Trypsin		
Sample	FCD from $[Na^+]$	FCD from $[Gd\text{-}DTPA^{-2}]$	Ratio of FCDs	FCD from $[Na^+]$	FCD from $[Gd\text{-}DTPA^{-2}]$	Ratio of FCDs
A2	-0.331	-0.158	0.478	-0.006	-0.022	3.515
A3	-0.367	-0.180	0.492	0.075	-0.011	-0.149
B2	-0.330	-0.127	0.385	0.020	0.001	0.058
B3	-0.336	-0.148	0.441	0.028	-0.010	-0.376
B4	-0.412	-0.180	0.438	0.017	0.001	0.046
		Average:	0.447			
		Std. Dev.:	0.042			

Table 5.1: Shown here are the FCDs, in moles/liter (M) of five cartilage samples both before and after treatment with trypsin. Before the treatment, as expected form the results of Bashir et al [7], the average of the ratio between FCDs calculated from Na^+ and from $Gd\text{-}DTPA^{-2}$ is equal to 0.447 and is within one standard deviation of 0.5. After treatment, no attempt was made to evaluate the ratio. The calculated fixed charge densities were, for many of the samples, actually positive values, which clearly indicates difficulties with measurement.

As the table shows, the FCDs calculated from ion concentrations measurements collected before treatment with trypsin follow the established pattern – the ratio of FCDs calculated using measurements of the two different ions is almost equal to ½. After treatment with trypsin, however, no attempt was made to generate an average. The calculated FCDs are, for some of the samples, actually positive values, which is impossible. Theoretically, with the loss of the charged proteoglycans, the concentrations of ions within the tissue should equal the concentrations of ions in the bath. Equation

2.7, which is used to calculate fixed charge density from ion measurements, is quite sensitive to minor changes in tissue ion concentration when tissue concentrations are equal to or less than bath concentrations. Small errors in measuring gadopentetate concentration, therefore, are reflected as large errors in the FCDs calculated. FCDs calculated from sodium are still more likely to incorporate error as NMR measurements of sodium in degraded cartilage suffer from visibility problems. Loss of proteoglycan from the cartilage matrix has the effect of lowering T_2. The loss of signal detection time makes it much harder to detect, with an NMR measurement, all the sodium that is present. Measurements that indicate tissue concentrations less than bath concentrations of sodium ions are probably due to this effect. Such measurements would lead to positive values calculated for FCD.

Note, however, that examination of Gd-DTPA^{-2} concentrations inside and outside the tissue shows them to be very similar. In Table 5.2, these concentrations, along with

Examination of [Gd-DTPA^{-2}] after Trypsin			
Sample	[Gd-DTPA^{-2}] in Bath	[Gd-DTPA^{-2}] in Tissue	Absolute Value of Tissue [Gd-DTPA^{-2}] - Bath [Gd-DTPA^{-2}]
A2	1.00E-03	8.63E-04	1.37E-04
A3	1.00E-03	9.28E-04	7.19E-05
B2	1.00E-03	1.01E-03	7.63E-06
B3	1.00E-03	9.33E-04	6.72E-05
B4	1.00E-03	1.01E-03	5.31E-06
		Average:	5.77E-05
		Std. Dev.:	5.43E-05

Table 5.2: Gadopentetate concentration in the five cartilage samples after degradation by trypsin was calculated from T_1 measurements. The difference between tissue and bath concentrations is shown here in the last column. Note that the average difference, while not actually equal to zero, is more than an order of magnitude smaller than the concentrations involved.

the absolute value of the difference in concentration, are tabulated. The lack of a significant difference suggests that the interior of the collagen fibers, which makes up a

larger portion of the total sample volume after removal of the proteoglycans, is accessible to the contrast agent.

5.2 Single Compartment Measurements

Having shown that gadopentetate appears to be distributed both inside and outside the collagen fibrils, attention was shifted to a proteoglycan only compartment. Since proteoglycans have no structural integrity, an imitation of the proteoglycan compartment was constructed as described in the methods (Section 4.2).

The concentrations of sodium and gadopentetate in the chondroitin sulfate solutions as determined from NMR measurements where used to calculate fixed charge density as outlined in section 4.3. After the NMR measurements were completed, a DMB assay was done to determine the actual amount of chondroitin sulfate present in each sample solution. FCD was determined from this biochemical data as described in section 4.4.

FCDs calculated by each of the three methods (from Na^+, from Gd-$DTPA^{-2}$, and from the DMB assay) are plotted against each other in Figure 5.1 and Figure 5.2. Figure 5.1 shows a plot of FCD from sodium measurements against FCD from gadopentetate measurements. In the absence of collagen, there is no second charge free compartment to cause deviations from the ideal Donnan system. Therefore, the slope of the regression line on this plot was expected to equal one, as predicted by Equation 2.7. As is immediately clear, the slope of the plotted relationship, 0.468, is nowhere near one, but quite close to 0.5. The factor of 2 seen in Figure 2.1, thought to exist because of water compartmentalization, continues to exist in a single compartment imitation of cartilage. The hypothesis stated in section 3.4 appears to have been disproved by this result.

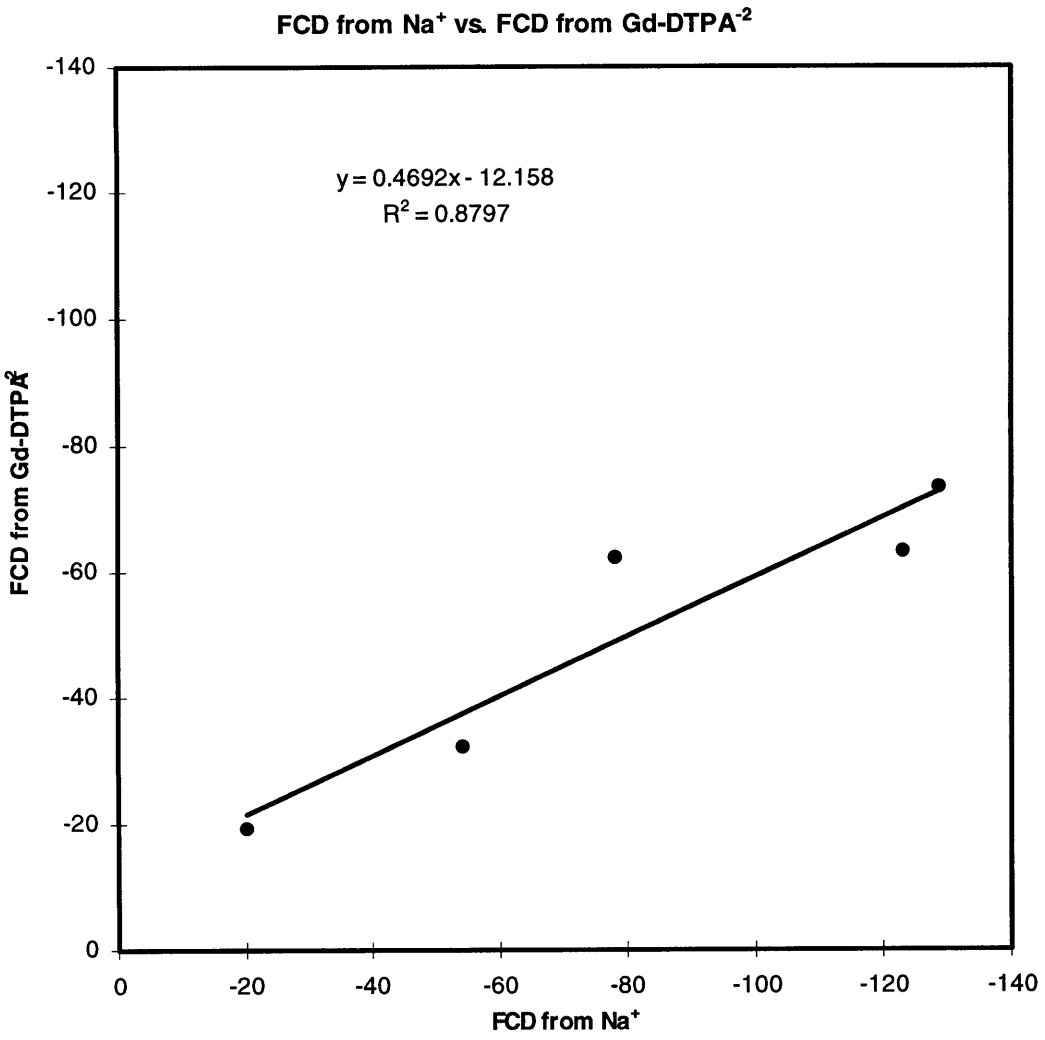

Figure 5.1: Plot of FCD as calculated from measurements of Na^+ concentration against FCD as calculated from measurements of Gd-DTPA^{-2} concentration. The data leading to these values of FCD were from NMR measurements of chondroitin sulfate solution that had been equilibrated in Hank's solution with Gd-DTPA^{-2}. Since there was no collagen present, the solution in dialysis bag construct should have been an ideal single compartment. Yet the regression line slope for these data is approximately 0.468 rather than the expected value of one.

The appearance of Figure 5.2 was a puzzle. Plotting FCD as calculated from sodium against FCD as calculated via biochemical methods yielded an unexpected result. The slope of the regression line between the two sets of data points is very close to ½. These two graphs posed interesting questions. Figure 5.1 appeared to clearly invalidate the original hypothesis. Yet the figures which follow immediately after suggest that

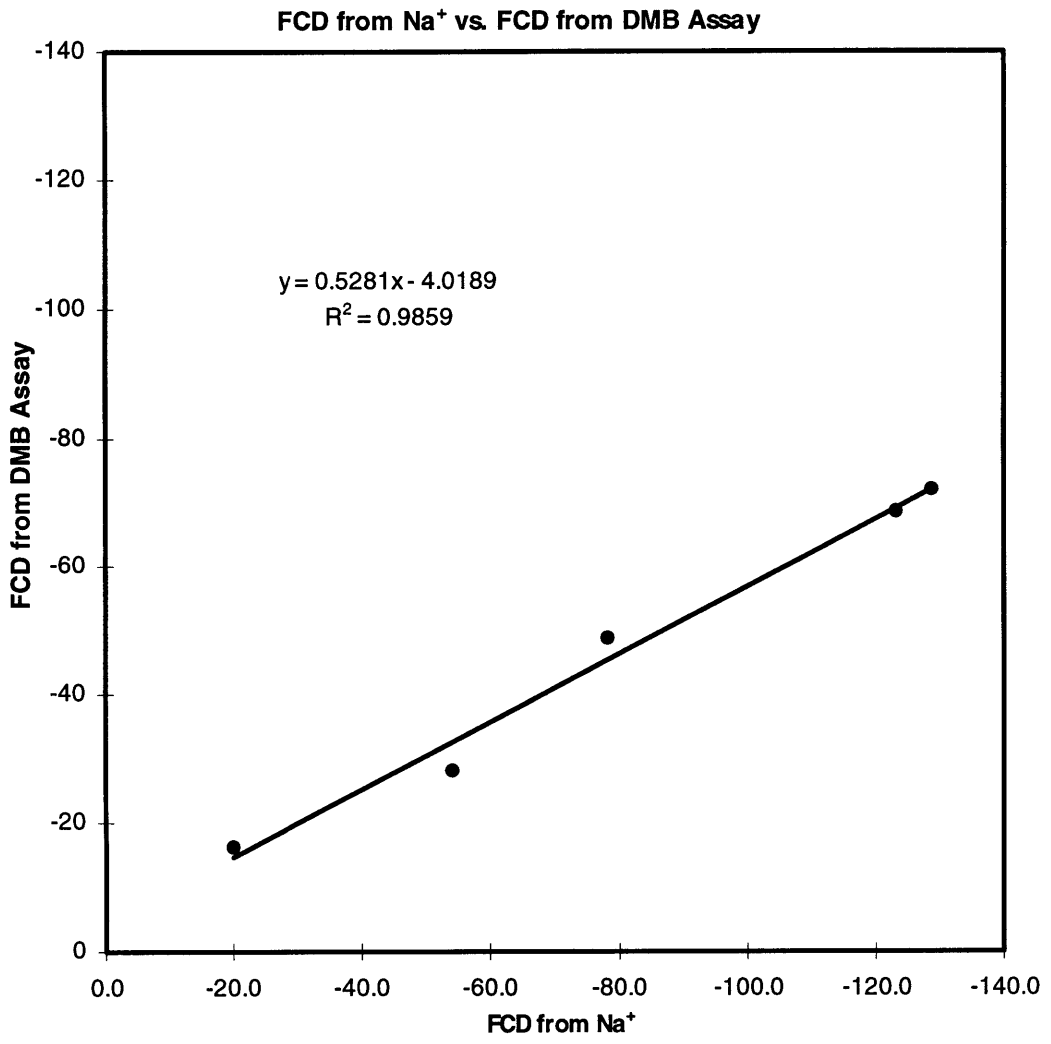

Figure 5.2: This graph plots FCD as calculated from measurements of Na^+ concentration against FCD as calculated from measurements of CS concentration via DMB. Unexpectedly, the slope of the regression curve here is 0.515. There is an apparent factor of two ratio between FCD from sodium and FCD from DMB. This lead to verification the Gd-DTPA-2 does not affect the DMB assay (Table 5.3). Ultimately, repetition of this particular comparison using data from other experiments refuted the suggestion that a factor of two ratio actually exists.

something odd has occurred. It has been shown that in cartilage, FCD as calculated from sodium measurements does correctly predict the fixed charge density [47]. The last figure seemed to suggest that this may not hold true for simple chondroitin sulfate solutions. Since, as noted previously, the chondroitin sulfate used for the DMB assay standards comes from the same source as the CS in the samples, there is little chance of

hidden **Error! Bookmark not defined.** in the assay procedure. Calculation of FCD from the concentration of CS so calculated is a very simple and routine process, again leaving little room for a hidden error. The only obvious possibility as a source of error was the inclusion of gadopentetate in the solutions assayed using DMB. Any chemical reactions between the cationic dye and the anionic gadopentetate could affect the final result.

Samples in Various Gd-DTPA^{-2} Concentrations								
[Gd-DTPA^{-2}] (mM)	25	10.00	1	0.1	0.01	0	Ave	Std Dev
Actual [CS] (µg/ml)	537.5	537.5	537.5	537.5	537.5	537.5		
[CS] from DMB (µg/ml)	581.2	573.6	570.3	584.5	563.8	575.8		
DMB [CS] / Actual [CS]	1.08	1.07	1.06	1.09	1.05	1.07	1.07	0.01

Table 5.3: Ratio of CS concentration measured via DMB to actual CS concentration. Although the [CS] calculated from DMB is at least 5% greater than the known [CS] of each sample, note that the same holds true for the 0mM [Gd-DTPA^{-2}] solution. This means that the 5% difference is likely to be measurement or calculation error, having no significance as far as the effect of gadopentetate upon the DMB assay. In fact the standard deviation for these samples is only 1%.

At first glance, Table 5.3 appears to show that there is some interaction between gadopentetate and the DMB. All the concentration calculated from measurement are at least 5% greater than the known concentrations. The 0mM gadopentetate solution also shows this shows the same results, however, suggesting that the observed difference is due to measurement or standardization error, rather than to any effect of the gadopentetate. Therefore, the gadopentetate does not appear to have an effect on the DMB measurements. (Even if some interaction is hidden within that 5% region, the results depicted in Figure 5.2 would require effects on the order of 50%.)

Since the factor of two relationship observed between FCD calculated from sodium and FCD calculated from the DMB assay did not seem to be a result of the DMB

assay, the only avenue left for error was the NMR measurement process. The experiment was, therefore, repeated, and the results are plotted in Figure 5.3 and Figure 5.4.

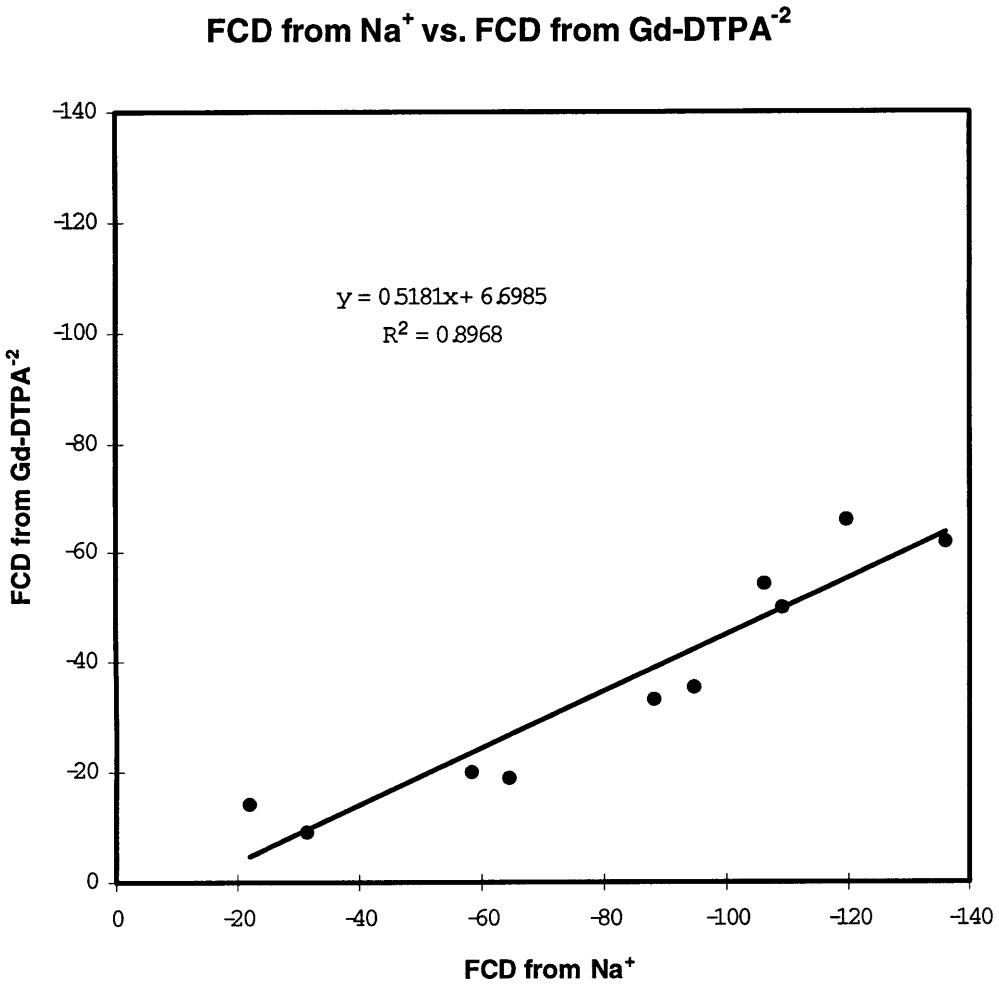

Figure 5.3: Another plot of FCD as calculated from measurements of Na^+ concentration against FCD as calculated from measurements of Gd-$DTPA^{-2}$ concentration. The data leading to these values of FCD were from a second set of NMR measurements of chondroitin sulfate solution that had been equilibrated in Hank's solution with Gd-$DTPA^{-2}$. The regression line slope for these data is approximately 0.5181. The factor of two relationship here remains as in the previous experiment.

As before, the slope of the regression line between FCD calculated from measurements of sodium concentration and measurements of gadopentetate concentration are related by a factor of two. Once again, the hypothesis has been disproved.

The line relating FCD from sodium measurements to FCD from the DMB assay, however, now has a different slope, 1.0962, much closer to one than its former 0.5821. This suggests that at least one of the two measurements is the result of an error. Further data would be useful to determine which is more likely to be correct.

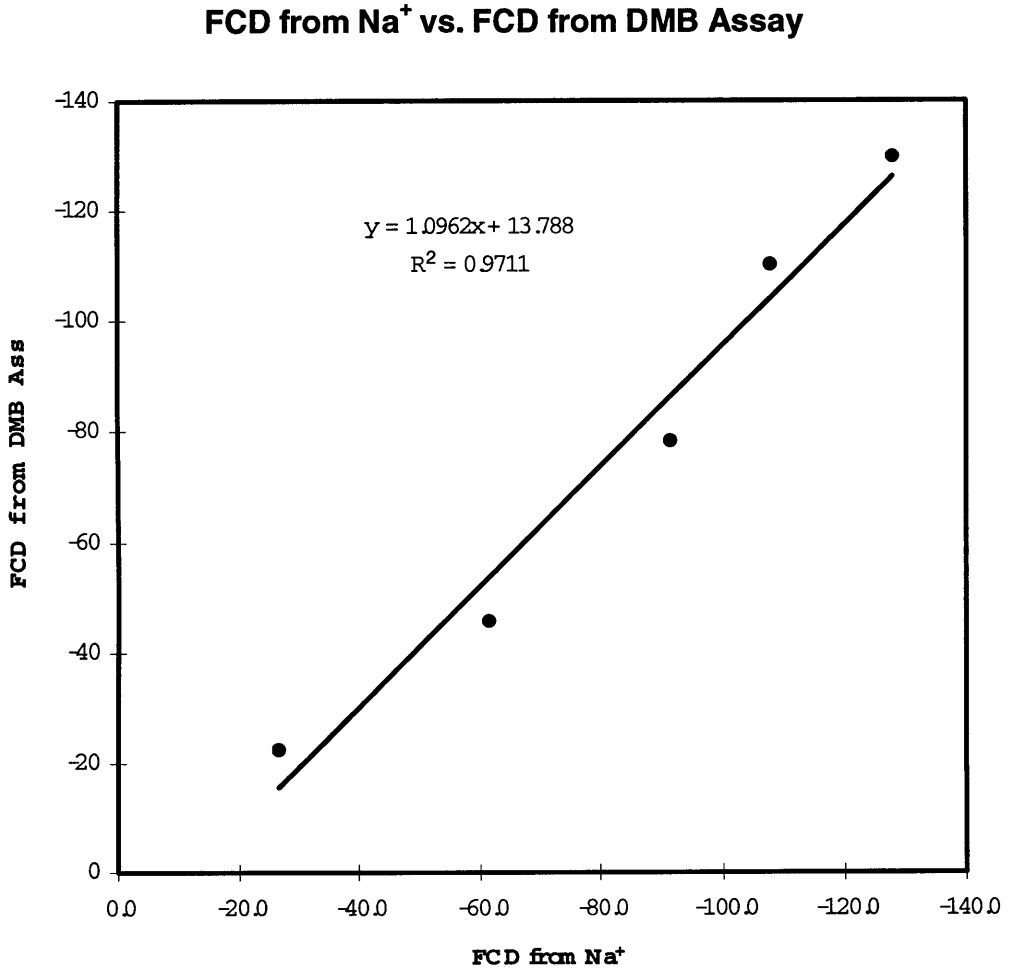

Figure 5.4: A second plot of FCD from sodium measurements against FCD from the DMB assay. Unlike the last time (Figure 5.2), the slope of the regression line is approximately equal to one, providing support for the idea that the previous set of measurements was somehow skewed by a factor of two during the experiment.

5.3 Steric Effect Measurement

From Figure 5.1 and Figure 5.3, it appeared clear that the factor of two observed by Bashir et al was not due primarily to regions with different fixed charge. The possibility existed, however, that steric exclusion might be causing the formation of two regions of differing ion concentration. The gadopentetate molecule, as shown in Figure 2.11, is a large organometallic complex. The sodium ion, on the other hand, is a single atom (MW = 23.0g/mol). It is conceivable that there might exist regions accessible to the small sodium ion but inaccessible to a large complex.

To test this hypothesis, the chondroitin sulfate solution dialysis experiments were repeated two more times. This time, however, a *non-ionic* gadolinium based contrast agent (ProHance – Gd-HP-DO3A) was used instead of Gd-DTPA^{-2}. ProHance, like gadopentetate, is a fairly large organometallic coordination compound. Obviously, there is no expected correlation between the existence of fixed charge and ProHance concentration. ProHance concentration in all samples, regardless of CS concentration, should be the same as in the bath. If steric exclusion is a factor, however, then ProHance concentration in samples should decrease with increasing CS concentration.

In Figure 5.5, the concentrations of Na^+ and ProHance found in the samples is normalized with respect to bath concentrations and plotted. Concentrations of Na^+ show a clear correlation with fixed charge density. The negative increase of FCD implies a greater concentration of sodium. ProHance concentrations, at low FCDs, are almost the same in the samples and in the bath. Further, the values stay fairly constant over small changes in FCD. At higher FCDs, however, the ProHance in the samples apparently increases, acting somewhat like a positive ion. Although only one set of data is presented

here, both of the experiments using ProHance displayed this apparent concentration increase in samples at higher FCDs. Steric exclusion, as explained before, would result not in an increase in average concentration, but rather in a decrease.

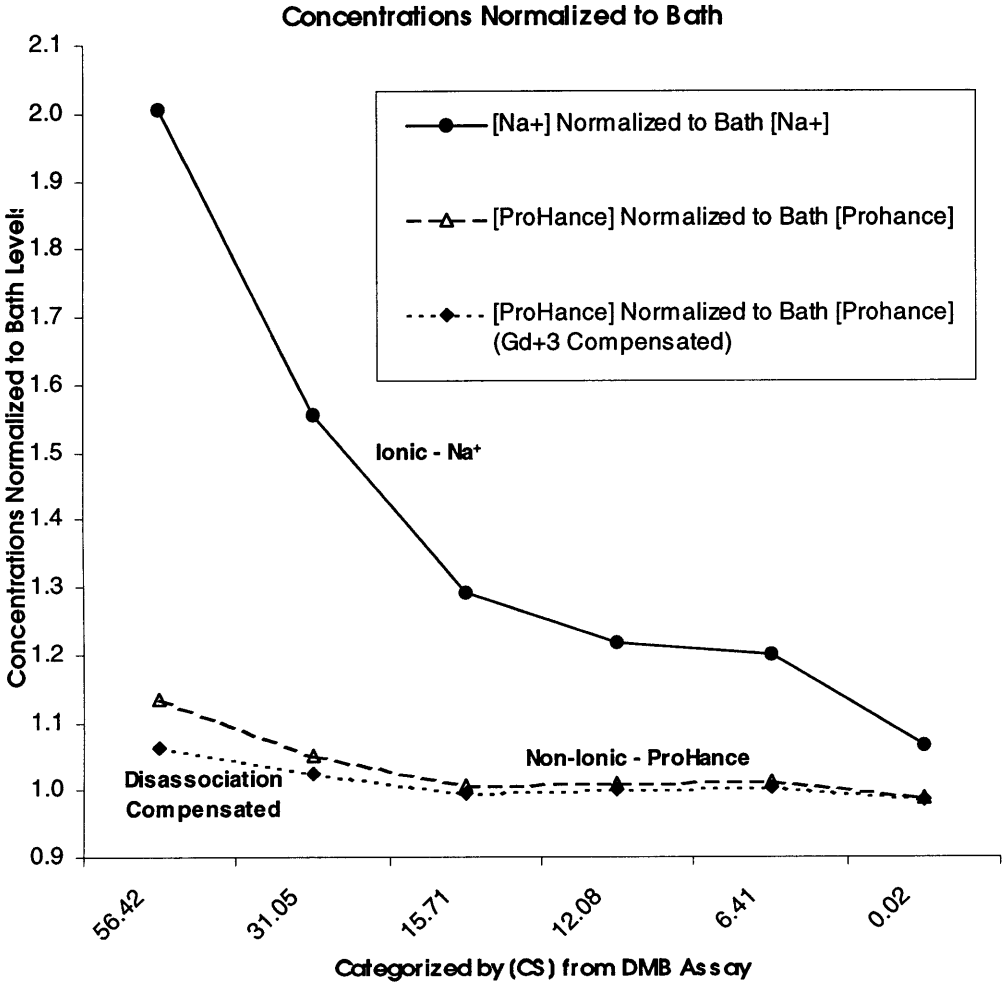

Figure 5.5: This figure shows concentrations of sodium and ProHance in the dialysis bags normalized to concentrations outside. As expected from Donnan considerations, the concentration of sodium inside increases with respect to the outside as fixed charge density increases. At low FCDs, [ProHance] behaves exactly like a non-ionic material is expected to behave under Donnan equilibrium: the normalized concentration is about equal to 1, and is fairly constant with fixed charge density. At higher FCDs, however, the ProHance concentration actually appears to increases in the sample. (Steric exclusion would suggest a decrease.) The "Disassociation Compensated" curve on the graph represents an attempt at explaining the apparent increase in sample [ProHance]. Disassociated Gd^{+3} could significantly alter the T_1s used to calculate [ProHance]. The curve represents [ProHance] corrected for a 1% disassociation.

One possible explanation for the apparent increase was the link between T_1 and ProHance concentration. Since the value actually measured is T_1, any other element which alters T_1 would alter the calculated values of ProHance concentration. If the ProHance metal complex is partially disassociated, permitting some free Gd^{+3} ions in the bath, there would be a T_1 effect associated with the free metal rather than with ProHance. Further the cationic nature of Gd^{+3} would cause concentrations in the samples to increase with the negatively increasing FCD.

Theoretically, it is possible to solve, using Donnan, for the concentration of Gd^{+3} in each sample if the bath concentration of the ion is known.

$$\left(\frac{\bar{c}_{Na^+}}{c_{Na^+}}\right)^3 = \frac{\bar{c}_{Gd^{+3}}}{c_{Gd^{+3}}}$$

$$\bar{c}_{Gd^{+3}} = c_{Gd^{+3}}\left(\frac{\bar{c}_{Na^+}}{c_{Na^+}}\right)^3$$

Given this solution, assuming that the Gd^{+3} ion has the same relaxivity as ProHance, and assuming that ProHance undergoes 1% spontaneous disassociation, the observed curve can be redrawn in Figure 5.5 after compensating for the presence of Gd^{+3}. As can be seen in the figure, the line formed by the compensated points does not turn upward as sharply as that formed by the uncompensated figures. Complete correction is unlikely to be observed, even if this were the correct explanation, due to the two assumptions made above. (The relaxivity of free Gd^{+3} in water has, in fact, been shown to be about three times the relaxivity of ProHance at 20MHz [73,45,28], which suggests that only a third as much disassociation is needed to achieve the error observed. Unfortunately, it is not possible to incorporate this information in plotting the compensated curve since, if disassociation occurs, the relaxivity calculated for ProHance

already incorporates the contribution of some free Gd^{+3}. This leads to more unknowns – concentrations inside tissue and their relationships – than there are equations to describe the system.)

Since the data from this second set of experiments (using a non-ionic agent) partially repeated the data from the experiments with gadopentetate, Figure 5.6 and Figure 5.7 were generated to aid with the puzzle posed by Figure 5.2.

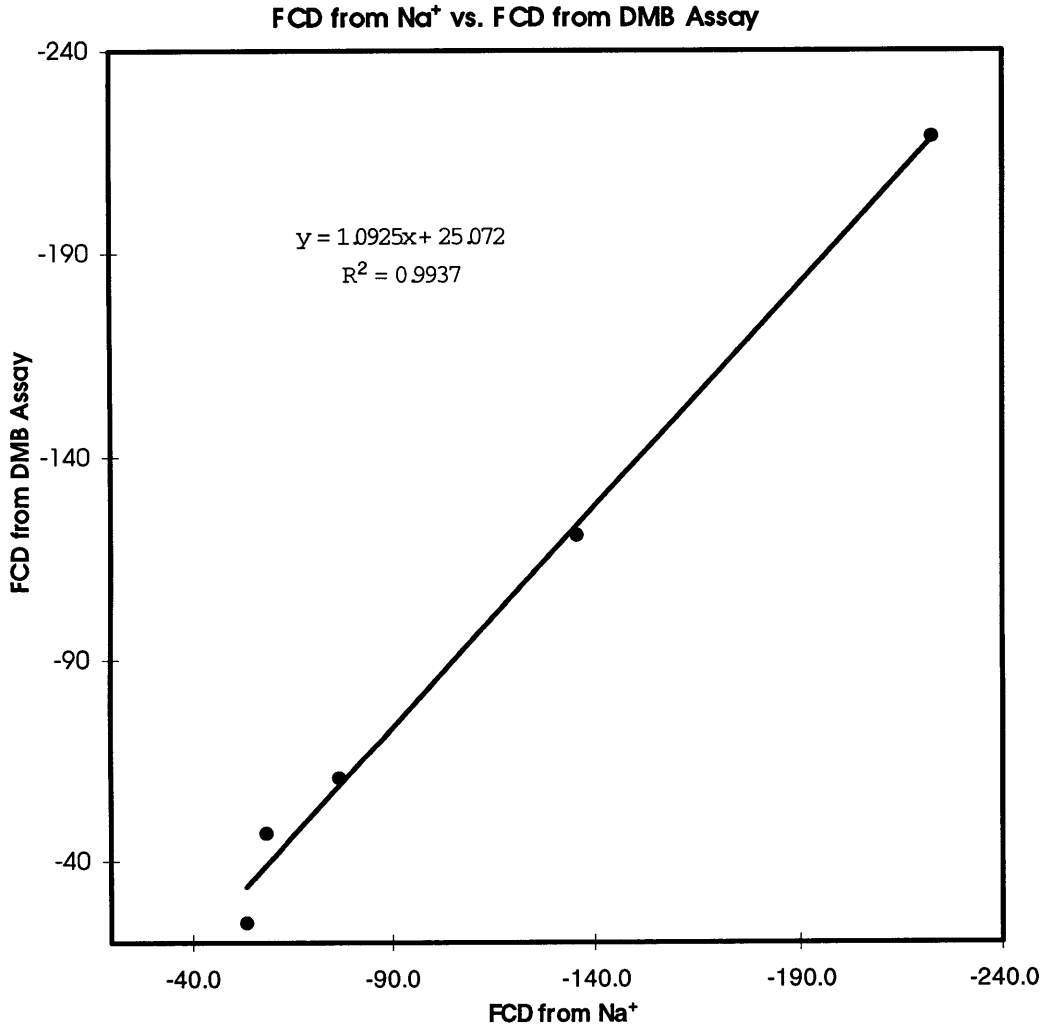

Figure 5.6: This graph plots FCD as calculated from measurements of Na^+ concentration against FCD as calculated from measurements of CS concentration via DMB. The observed slope of the regression line here is 1.09, very close to 1.

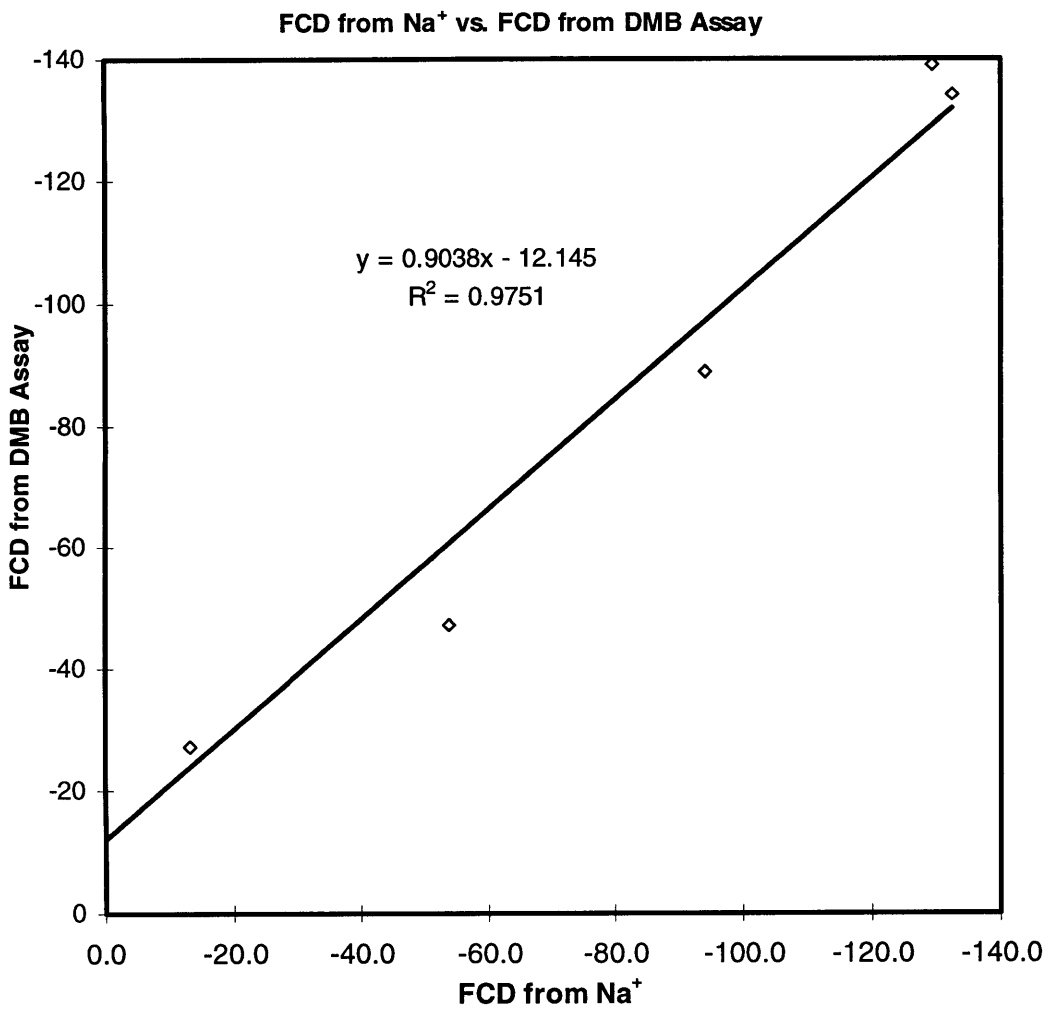

Figure 5.7: This graph, representing a fourth experiment, also depicts FCD from sodium against FCD from the DMB assay. Here, although there is a greater spread of the points, the slope of the line is again near one (1), at 0.90.

Unlike Figure 5.2, which plotted exactly the same variables for the experiment with gadopentetate, the slope of the regression curves in these new figures are about equal to 1. The only purposeful difference between the two experiments was the substitution of ProHance for gadopentetate. This substitution offers no immediate explanation for the problem that Figure 5.2 poses. Considering that repetition of the experiment with gadopentetate (Figure 5.4) also led to a similar curve with a slope of about one, the simplest explanation suggests that a procedural experimental error scaled

all values by a factor of two and that – as illustrated by Figure 5.4, Figure 5.6 and Figure 5.7 – there is a close correspondence between FCD determined from sodium concentration measurements and FCD determined by the biochemical DMB assay .

Chapter 6: Conclusion

6.1 Summary

Experimental work published by Lesperance et al. [47] demonstrated that cartilage fixed charge could be monitored *in vitro* by NMR measurements of sodium ion signal within the tissue. Bashir et al. [7] continued with this work to show that use of a charged contrast agent, gadopentetate (Gd-DTPA^{-2}), and measurements of proton T_1 provided another route to the same end.

Both methods made use of Donnan equilibrium theory to evaluate fixed charge. Interestingly, the final value of fixed charge calculated from sodium measurements was generally twice the value calculated from gadopentetate measurements. The model in use at the time provided no explanation for this discrepancy.

It had long been known that the water content of cartilage was divided between two physiologically distinct regions [51]: the intrafibrillar region within each collagen fibril, and the extrafibrillar region, which contains all the tissue fixed charge. One possible theoretical explanation for the observed discrepancy in calculations of fixed charge, therefore, suggested that the model used in Donnan calculations be modified to consist of two compartments, in which all the tissue fixed charge is located in one compartment.

Explorations of this model (section 3.1) did account neatly for the discrepancy.

If the theoretical explanation was an accurate description of the situation within cartilage, then it was hypothesized that either one of the two compartments, if isolated and submitted to the same sorts of NMR measurements, would show no discrepancy between the calculated values of FCD.

To this end, an attempt was first made to examine the intrafibrillar compartment by working with cartilage exposed to trypsin. Unfortunately, although the results of the experiment did suggest that gadopentetate was entering the GAG free cartilage completely, problems with low sodium visibility at low fixed charge densities made the experiment impractical.

The extrafibrillar compartment, though not directly isolatable, was imitated by solutions of chondroitin sulfate. Measurements were successfully made on samples with varying fixed charge. When tissue fixed charge density was calculated from these measurements, a discrepancy was once again observed. Calculations of FCD in single compartment chondroitin sulfate solutions using measurements of gadopentetate concentration yielded values about 50% less than similar calculations based on sodium concentration measurements or on biochemical assays. The hypothesis had failed.

Further explorations were done to determine if steric exclusion effects could provide an explanation. To this end, measurements were made using an uncharged contrast agent (ProHance). In an ideal Donnan single compartment, any uncharged agent would be unaffected by fixed charge. It would diffuse until concentrations within the sample equaled concentration outside the sample. Steric exclusion, however, would mean that the average concentration of ProHance would decrease as the excluded volume increased. It was observed that for low fixed charges, ProHance behaved exactly as expected, diffusing until reaching bath concentrations within the sample. For higher fixed charge densities, however, the amount of ProHance in the sample was seen to increase. One possible explanation, supported by theoretical analysis, is that the

ProHance organometallic complex was partially disassociated, freeing gadolinium(3+) to affect the measurements.

6.2 Future Work

Since this work has shown that the proposed hypothesis failed, a reason for the factor of two discrepancy which motivated this work remains to be found. Not only must it be explained within cartilage, but also within simpler models like the chondroitin sulfate suspensions developed here. Possibilities include:

(a) that the gadopentetate contrast agent, because of its large size and complicated organomettalic structure allowing shielding of charge, could be better described as behaving like a molecule with a –1 rather than a –2 charge.

(b) that a small fraction of the gadolinium is disassociated from the gadopentetate complex, leading to free Gd^{+3} ions in the solution.

(c) that Donnan theory is inadequate to describe the average concentration of a divalent ion in a charged matrix as the Donnan model neglects the complex spatial distribution of the mobile ions. .

In the light of these ideas, it would be particularly useful, from a basic science perspective, to explore the distribution of other mono- and di- valent ions (both anions and cations) in simple Donnan single compartment solutions. If shielding is a factor, then less complex ions should result in measurements that do match with Donnan theory. Exploration of Donnan single compartment models other than chondroitin sulfate solutions could provide an avenue of research. Gels or solutions with a positive rather than a negative fixed charge will lead to new insight into ion distribution behavior in cartilage.

Further, since cartilage is physiologically composed of two different regions, it remains to be determined what effect compartmentalization does have upon ion distribution in tissue. As mentioned before, it has been shown that cartilage fixed charge density is well described by measurements using sodium NMR. Yet, given the compartmentalization of the tissue, there must be some error associated with these measurements. A quantification of that error as a function of measured fixed charge would be useful, permitting empirical calculation of true fixed charge density from the sodium NMR based values.

On a larger screen, gadopentetate studies are already being explored as a means of monitoring proteoglycan loss *in vivo*. Better understanding of the diffusion and clearance of contrast agents from the body is needed. Development and exploration of other charged contrast agents for use in a similar manner would be useful as well.

The potential for early diagnosis provided by gadopentetate based methods currently being developed could soon permit a better understanding of disease onset, and permit the development of early treatments. Hopefully, a few years from now, MRI examination of cartilage condition will become a regular part of the yearly checkup. The potential savings in money and in pain are huge.

Appendix A: Example of 2 Compartment FCD Derivation

Figure 3.1 and Figure 3.2 attempt to convey how the ratio between FCD calculated from Gd-DTPA^{-2} (FCD calculated from Cl^- concentration in the case of Figure 3.2) and FCD calculated from Na^+ concentration would be affected by extrafibrillar compartment volume. The curves on the figures were derived assuming that although a single compartment Donnan model is used for FCD calculations, the appropriate description of the system is a two-compartment model.

In this appendix, the mathematical procedure used to derive each point on the curve will be demonstrated via a specific example. Since the process is almost identical for both gadopentetate and chlorine, the example will cover only the gadopentetate case.

First, we choose some useful bath concentrations, an initial "calculated" FCD, and an extrafibrillar volume fraction of interest. Suppose:

$$\begin{aligned} v_{EF} &= 0.50 \\ c_{Na^+} &= 150\,\text{mM} \\ c_{Cl^-} &= 150\,\text{mM} \\ \text{FCD}_{Na^+} &= \text{FCD from } \bar{c}_{M_{Na^+}} = -200\,\text{mM} \end{aligned}$$

Beginning with the assumed value for the FCD, the volume-averaged concentration of Na^+ is calculated using Equation 2.7.

$$\begin{aligned} \text{FCD} &= \frac{c_{Na^+}^2}{\bar{c}_{M_{Na^+}}} - \bar{c}_{M_{Na^+}} \\ (\text{FCD})\bar{c}_{M_{Na^+}} &= c_{Na^+}^2 - c_{M_{Na^+}}^2 \\ c_{M_{Na^+}}^2 + (\text{FCD})\bar{c}_{M_{Na^+}} - c_{Na^+}^2 &= 0 \\ \bar{c}_{M_{Na^+}} &= \frac{-\text{FCD} \pm \sqrt{(\text{FCD})^2 + 4c_{Na^+}^2}}{2} \end{aligned}$$

Substituting the values suggested above, the volume-averaged concentration of Na^+ is found to be 280.28 mM. Next, substitution into Equation 3.3 permits determination of the actual concentration of Na^+ in the extrafibrillar compartment.

$$\bar{c}_{M_{Na^+}} = c_{Na^+}(1-v_{EF}) + \bar{c}_{Na^+}v_{EF}$$

$$\bar{c}_{Na^+}v_{EF} = \bar{c}_{M_{Na^+}} - c_{Na^+}(1-v_{EF})$$

$$\bar{c}_{Na^+} = \frac{\bar{c}_{M_{Na^+}} - c_{Na^+}(1-v_{EF})}{v_{EF}}$$

Once again substituting values shows that the actual concentration of sodium in the extrafibrillar volume is 410.56 mM. Now, the Donnan equilibrium, as outlined in Equation 2.4, leads to concentration of Gd-$DTPA^{-2}$ in the extrafibrillar compartment.

$$\frac{\bar{c}_{Na^+}}{c_{Na^+}} = \left(\frac{c_{Gd\text{-}DTPA^{-2}}}{\bar{c}_{Gd\text{-}DTPA^{-2}}}\right)^{1/2}$$

$$\bar{c}_{Gd\text{-}DTPA^{-2}} = \left(\frac{c_{Na^+}}{\bar{c}_{Na^+}}\right)^2 c_{Gd\text{-}DTPA^{-2}}$$

Substitution leads to a value for extrafibrillar gadopentetate concentration: 0.13 mM. Now Equation 3.3 comes into play once more to determine the volume averaged gadopentetate concentration.

$$\bar{c}_{M_{Gd\text{-}DTPA^{-2}}} = c_{Gd\text{-}DTPA^{-2}}(1-v_{EF}) + \bar{c}_{Gd\text{-}DTPA^{-2}}v_{EF}$$

Recalling the chosen value of v_{EF}, 0.50, from above, and substituting the gadopentetate concentration calculated previously, the volume-averaged concentration is found to be 0.57 mM. Finally, using Equation 2.7, FCD is calculated from the volume averaged gadopentetate concentration.

$$FCD_{Gd\text{-}DTPA^{-2}} = \text{FCD from } \bar{c}_{M_{Gd\text{-}DTPA^{-2}}} = c_{Na^+}\left(\sqrt{\frac{\bar{c}_{M_{Gd\text{-}DTPA^{-2}}}}{c_{Gd\text{-}DTPA^{-2}}}} - \sqrt{\frac{c_{Gd\text{-}DTPA^{-2}}}{\bar{c}_{M_{Gd\text{-}DTPA^{-2}}}}}\right)$$

A last substitution gives shows that, as calculated from a volume-averaged Gd-DTPA-2 concentration, the FCD is only -86.33 mM. The ratio plotted in Figure 3.1 is the ratio of this value to the originally chosen value: (-86.33)/(-200) = 0.43.

In concluding, it is important to note that this derivation could also have been done by choosing a volume averaged fixed charge density, determining the FCD in the extrafibrillar compartment, and continuing on to determine the volume averaged concentrations of sodium and gadopentetate. Once those values are known, FCD could be calculated separately for the two ions, and the same ratio obtained. It was decided to take the approach actually outlined in example above for several reasons. First of all, exactly the same curves can be generated with both processes by choosing the initial value of FCD appropriately. Given that the same curves are generated, it seemed more practical to select the derivation method that involved fewer steps and corresponds more closely to the types of observations actually presented in this work (fixed charge densities calculated from volume averaged ion measurements). Finally, the issue of the relationship between the volume averaged fixed charge density and the fixed charge density calculated from volume averaged ion concentrations is dealt with separately by in section 3.3.

Appendix B: Calculation of Extrafibrillar Volume

Equation 2.1 and Equation 3.3 expressed for particular ions, together provide a system of equations that can be solved to derive an expression for the volume fraction of water, v_{EF}, in the extrafibrillar compartment of cartilage in terms of known or measurable ion concentrations. Below, this derivation will be performed to express v_{EF} in terms of Na^+ and Cl^- concentrations, as well as in terms of Na^+ and Gd-DTPA^{-2} concentrations.

The derivations below assume a couple of points. First, it is assumed that each of the two compartments (extrafibrillar and intrafibrillar) satisfy the Donnan model at equilibrium. This means that concentrations of ions in the intrafibrillar regime (where no fixed charge exists) will be equal to concentrations of ions in the external bath. Ion concentrations in the extrafibrillar region are assumed to be well described by Equation 2.1. Second, it is assumed that the external bathing solution has equal concentrations of Na^+ and Cl^-. It is possible to perform the derivation assuming different concentrations but it is not nearly as neat or easy to follow.

B.1. Na^+ and Cl^-

First of all, the specific parameters which are known must be identified. When considering a sodium and chloride system:

$\overline{C}_{M_{Na^+}} \equiv$ average concentration of Na^+ : determined from measurement.

$\overline{C}_{M_{Cl^-}} \equiv$ average concentration of Cl^- : determined from measurement.

$C_0 \equiv$ concentration of Na^+ and Cl^- in the external solution.

Substituting as appropriate into Equation 2.1 and Equation 3.3, the following initial relationships are found:

$$\overline{C}_{M_{Na^+}} = C_0(1-v_{EF}) + \overline{C}_{Na^+} v_{EF}$$

Equation 6.1

$$\overline{C}_{M_{Cl^-}} = C_0(1-v_{EF}) + \overline{C}_{Cl^-} v_{EF}$$

Equation 6.2

$$\frac{\overline{C}_{Na^+}}{C_0} = \frac{C_0}{\overline{C}_{Cl^-}}$$

Equation 6.3

Immediately, it is clear from Equation 6.3 that:

$$\overline{C}_{Cl^-} = \frac{C_0^2}{\overline{C}_{Na^+}}$$

Substituting into Equation 6.2 and solving for the concentration of Na^+ results in:

$$\overline{C}_{M_{Cl^-}} = C_0(1-v_{EF}) + \frac{C_0^2 v_{EF}}{\overline{C}_{Na^+}}$$

$$\overline{C}_{Na^+} = \frac{C_0^2 v_{EF}}{\overline{C}_{M_{Cl^-}} - C_0(1-v_{EF})}$$

Now substituting a final time into Equation 6.1 leads to an equation that can be quickly solved.

$$\overline{C}_{M_{Na^+}} = C_0(1-v_{EF}) + \frac{C_0^2 v_{EF}}{\overline{C}_{M_{Cl^-}} - C_0(1-v_{EF})} v_{EF}$$

This expression looks fairly complicated, including some second order terms, but those terms cancel out after cross multiplication, resulting in a solution for v_{EF} that includes only those terms which were earlier identified as known.

$$v_{EF} = \frac{\left(C_0 - \overline{C}_{M_{Na^+}}\right)\left(C_0 - \overline{C}_{M_{Cl^-}}\right)}{C_0\left(2C_0 - \overline{C}_{M_{Na^+}} - \overline{C}_{M_{Cl^-}}\right)}$$

Equation 6.4

B.2. Na^+ and Gd-$DTPA^{-2}$

A similar process can be followed for the sodium and gadopentetate system. First, known parameters are identified:

$\overline{C}_{M_{Na^+}}$ ≡ average concentration of Na^+ : determined from measurement.

$\overline{C}_{M_{Gd\text{-}DTPA^{-2}}}$ ≡ average concentration of Gd - $DTPA^{-2}$: determined from measurement.

C_0 ≡ concentration of Na^+ in the external solution.

C_G ≡ concentration of Gd - $DTPA^{-2}$ in the external solution.

Returning to Equation 2.1 and Equation 3.3, the initial relationships are identified. One of those relationships is expressed by Equation 6.1, as sodium is still a component. An equivalent relationship is found for gadopentetate, the Donnan equilibrium expression is identified and substitutions are made as appropriate.

$$\overline{C}_{M_{Gd\text{-}DTPA^{-2}}} = C_G(1-\nu_{EF}) + \overline{C}_{Gd\text{-}DTPA^{-2}}\nu_{EF}$$

Equation 6.5

$$\left(\frac{\overline{C}_{Na^+}}{C_0}\right)^2 = \frac{C_G}{\overline{C}_{Gd\text{-}DTPA^{-2}}}$$

Equation 6.6

Equation 6.6, once reformulated, gives:

$$\overline{C}_{Gd\text{-}DTPA^{-2}} = \left(\frac{C_0}{\overline{C}_{Na^+}}\right)^2 C_G$$

Substituting in Equation 6.5 and attempting to solve for the concentration of Na^+ results in:

$$\overline{C}_{M_{Gd\text{-}DTPA^{-2}}} = C_G(1-\nu_{EF}) + \left(\frac{C_0}{\overline{C}_{Na^+}}\right)^2 C_G\nu_{EF}$$

$$\overline{C}^2_{Na^+} = \frac{C_0^2 C_G \nu_{EF}}{\overline{C}_{M_{Gd\text{-}DTPA^{-2}}} - C_G(1-\nu_{EF})}$$

In order to avoid dealing with square roots, it makes sense to manipulate Equation 6.1 somewhat as shown:

$$\bar{c}_{M_{Na^+}} = c_0(1-v_{EF}) + \bar{c}_{Na^+} v_{EF}$$

$$\bar{c}^2_{Na^+} = \left[\frac{\bar{c}_{M_{Na^+}} - c_0(1-v_{EF})}{v_{EF}}\right]^2$$

Setting the two expressions for the square of Na^+ concentration equal to each other and manipulating the resulting equation results in an final equation of a very familiar form.

$$\frac{c_0^2 c_G v_{EF}}{\bar{c}_{M_{Gd-DTPA^{-2}}} - c_G(1-v_{EF})} = \left[\frac{\bar{c}_{M_{Na^+}} - c_0(1-v_{EF})}{v_{EF}}\right]^2$$

$$Av_{EF}^2 + Bv_{EF} + C = 0$$

where

$$A = c_0^2\left(\bar{c}_{M_{Gd-DTPA^{-2}}} - c_G\right) + 2c_0c_G\left(\bar{c}_{M_{Na^+}} - c_0\right)$$

$$B = 2c_0c_G\left(\bar{c}_{M_{Na^+}} - c_0\right)\left(\bar{c}_{M_{Gd-DTPA^{-2}}} - c_G\right) + c_G\left(\bar{c}_{M_{Na^+}} - c_0\right)^2$$

$$C = \left(\bar{c}_{M_{Na^+}} - c_0\right)^2\left(\bar{c}_{M_{Gd-DTPA^{-2}}} - c_G\right)$$

In this case, the third order terms cancelled out leaving a quadratic. The final solutions are then easily determined by the quadratic formula. The last step is choosing between the two possible solutions. That choice must be made to ensure that the value calculated for v_{EF} lies between 0 and 1 – as it represents the volume fraction of extrafibrillar water – and is not further addressed here.

$$v_{EF} = \frac{-B \pm \sqrt{B^2 - 4AC}}{2A}$$

Equation 6.7

Bibliography

1. Anonymous. "Nuclear Magnetic Resonance Spectroscopy: Theoretical Principles." WWW Site: http://www.shu.ac.uk/schools/sci/chem/tutorials/molspec/nmr1.htm. Sheffield Hallam University School of Science and Mathematics. UK.
2. Bacic, Goran et al. "MRI Contrast Enhanced Study of Cartilage Proteoglycan Degradation in the Rabbit Knee." *Magnetic Resonance in Medicine.* 37:764-768. 1997.
3. Ballinger, R. "MRI Tutor." WWW Site: http://128.227.164.224/mritutor/index.html. VA Medical Center. Gainsville, FL. 1998.
4. Bashir, A. "Sodium NMR Relaxation Parameters in Cartilage: Implications for MR Imaging." (S.M.Thesis.) Cambridge: MIT. 1995.
5. Bashir, A. et al. "Glycosaminoglycan in Articular Cartilage: In Vivo Assessment with Delayed Gd-$(DTPA)^{2-}$-enhanced MR Imaging." *Radiology.* 205:551-558. 1997.
6. Bashir, A. et al. "MRI of Glycosaminoglycan Distribution in Cartilage using Gd-$DTPA^{2-}$ In Vivo. In: *Proceedings of the Fifth Meeting of the International Society for Magnetic Resonance in Medicine.* Berkley, Calif: International Society for Magnetic Resonance in Medicine. p. 345. 1997.
7. Bashir, A., Gray, M.L. and Burstein, D. "Gd-$DTPA^{2-}$ as a Measure of Cartilage Degradation." *Magnetic Resonance in Medicine.* 36:665-673. 1996.
8. Bauer, W.R. and Schulten, K. "Theory of Contrast Agents in Magnetic Resonance Imaging: Coupling of Spin Relaxation and Transport." *Magnetic Resonance in Medicine.* 26:16-39. 1992.
9. Brittan, D. "A Window on Arthritis." *Technology Review.* 99:12-13. 1996.
10. Brown, M.A. "Effects of the Operating Magnetic Field on Potential NMR Contrast Agents." *Magnetic Resonance Imaging.* 3:3-9. 1985.
11. Brugières, P. et al. "Randomised Double Blind Trial of the Safety and Efficacy of Two Gadolinium Complexes (Gd-DTPA and Gd-DOTA)." *Neuroradiology.* 36:27-30. 1994.
12. Buckwalter et al. "Articular Cartilage: Composition and Structure." Park Ridge, IL: American Academy of Orthopaedic Surgeons. pp. 405-425. 1988.
13. Burstein, D. et al. "Diffusion of Small Solutes in Cartilage as Measured by Nuclear Magnetic Resonance (NMR) Spectroscopy and Imaging." *Journal of Orthopaedic Research.* 11:465-478. 1993.
14. Buschmann, M.D., Grodzinsky, A.J. "A Molecular Model of Proteoglycan-Associated Electrostatic Forces in Cartilage Mechanics." *Journal of Biomechanical Engineering.*117:189. 1995.
15. Bushong, Stewart C. *Magnetic Resonance Imaging Physical and Biological Principles.* Toronto: The C.V. Mosby Company. 1988.
16. Carney, S.L. and Muir, H. "The Structure and Function of Cartilage Proteoglycans." *Physiological Reviews.* 68: 858-910. 1988.
17. Carrington, A. and McLachlan, A.D. *Introduction to Magnetic Resonance.* London: Chapman and Hall. 1967.

18. Cho, Z.H., Jones, J.P. and Singh, M. *Foundations of Medical Imaging.* New York: John Wiley & Sons, Inc. 1993.

19. Comper, W.D. In: *Cartilage: Molecular Aspects.* Ed. B.K.Hall and S.A.Newman. Boston: CRC Press. pp. 59-96. 1991.

20. Dai, H., Potter, K., McFarland, E.W. "Determination of Ion Activity Coefficients and Fixed Charge Determination of Ion Activity Coefficients and Fixed Charge." *Journal of Chemical and Engineering Data.*41:970. 1996.

21. Donahue, K.M. "Studies of Gd-DTPA Relaxivity and Proton Exchange Rates in Tissue with Implications for MR Imaging of Regional Myocardial Perfusion." (Ph.D. Thesis.) Cambridge: MIT. 1986.

22. Donahue, K.M. et al. "Studies of Gd-DTPA Relaxivity and Proton Exchange Rates in Tissue." *Magnetic Resonance in Medicine.* 32:66-76. 1994.

23. Donahue, K.M., Weisskoff, R.M. and Burstein, D. "Water Diffusion and Exchange as They Influence Contrast Enhancement." *Journal of Magnetic Resonance Imaging.* 7:102-110. 1997.

24. Farndale, R.W., Buttle, D.J. and Barrett, A.J. "Improved Quantitation and Discrimination of Sulfated Glycosaminoglycans by use of Dimethylmethylene Blue." *Biochimica et Biophysica Acta.* 883: 173-177. 1986.

25. Farndale, R.W., Sayers, C.A. and Barrett, A.J. "A Direct Spectrophotometric Microassay for Sulfated Glycosaminoglycans in Cartilage Cultures." *Connective Tissue Research.* 9:247-248. 1982.

26. Frank, E.H. et al. "Physicochemical and Bioelectrical Determinants of Cartilage Material Properties." In: *Biomechanics of Diarthroidal Joints.* Ed. Van C. Mow, Anthony Ratcliffe and Savio L-Y. Woo. New York: Springer-Verlag. pp. 261-282. 1990.

27. Fullerton, G.D. "Physiological Basis of Magnetic Relaxation." In: *Magnetic Resonance Imaging.* 2nd edition. Ed. David D. Stark and William G. Bradley. Boston: Mosby Year Book. pp. 88-108. 1992.

28. Gore, J.C. and Brown, M.S. "Pathophysiological Significance of Relaxation." In: *Magnetic Resonance Imaging.* Ed. Partain, C.L. et al. Philadelphia: Saunders. pp. 1070-1074. 1988.

29. Gray, M.L. "Magnetization Transfer in Cartilage and Its Constituent Macromolecules." *Magnetic Resonance in Medicine.* 34:319-325. 1995.

30. Grodzinsky, A. Fields, Forces, and Flows in Biological Tissues and Membranes. Unpublished. Cambridge, MA: MIT. 1997.

31. Grodzinsky, A.J. "Electromechanical and Physiochemical Properties of Connective Tissue." *CRC Critical Reviews in Biomedical Engineering.* 9.2:133-199. 1983.

32. Hahn, E.L. "Spin Echoes." *Physical Review.* 80:580-594. 1950.

33. Hardingham, T.E. et al. "Cartilage Proteoglycans." *Functions of the Proteoglycans.* Chichester: Wiley. pp. 30-46. 1986.

34. Hendrick, R.E. and Haacke, E.M. "Basic Physics of MR Contrast Agents and Maximization of Image Contrast." *Journal of Magnetic Resonance Imaging.* 3:137-148. 1993.

35. Hinshaw, W. and Lent, A. "An Introduction to NMR Imaging: From the Bloch Equation to the Imaging Equation." *Proceedings of the IEEE.* 71:338-350. 1983.

36. Hodgson, R.J., Carpenter, T.A. and Hall, L.D. "Magnetic Resonance Imaging of Osteoarthritis." In: *Articular Cartilage and Osteoarthritis.* Ed. K. Kuettner et al. New York: Raven Press, Ltd. 1992.

37. Hornak, J.P. "The Basics of MRI." WWW Site: http://www.cis.rit.edu/htbooks/mri. Rochester Institute of Technology. Rochester, NY. 1997.

38. Hornak, J.P. "The Basics of NMR." WWW Site: http://www.cis.rit.edu/htbooks/nmr. Rochester Institute of Technology. Rochester, NY. 1997.

39. Jelicks, L.A. et al. "Hydrogen-1, Sodium-23, and Carbon-13 MR Spectroscopy of Cartilage Degradation in Vitro." *Journal of Magnetic Resonance Imaging.* 3:565-568. 1993.

40. Jones, J.P. "Physics of the MR Image: From the Basic Principles to Image Intensity." In: *Magnetic Resonance Imaging.* Ed. Partain, C.L. et al. Philadelphia: Saunders. pp. 1003-1027. 1988.

41. Jurvelin, J.S., Buschmann, M.D. and Hunziker, E.B. "Optical and Mechanical Determination of Poisson's Ratio of Adult Bovine Humeral Articular Cartilage." *J. Biomechanics.* 30:235-241. 1997.

42. Kanal et al. "Safety Considerations in MR Imaging." *Radiology.* 176:593-606. 1990.

43. King, K. and Moran, P. "A Unified Description of NMR Imaging, Data-Collection Strategies, and Reconstruction." *Medical Physics.* 11:1-14. 1984.

44. Koenig, S.H. and Brown, R.D. III. "Relaxometry of Solvent and Tissue Protons: Diamagnetic Contributors." In: *Magnetic Resonance Imaging.* Ed. Partain, C.L. et al. Philadelphia: Saunders. pp. 1035-1048. 1988.

45. Koenig, S.H. and Brown, R.D. III. "Relaxometry of Solvent and Tissue Protons: Paramagnetic Contributors." In: *Magnetic Resonance Imaging.* Ed. Partain, C.L. et al. Philadelphia: Saunders. pp. 1049-1069. 1988.

46. Kuettner, K.E. and Kimura, J.H. "Proteoglycans: An Overview." *Journal of Cellular Biochemistry.* 27: 327-336. 1985.

47. Lesperance, L.M., Gray, M.L. and Burstein, D. "Determination of Fixed Charge Density in Cartilage Using Nuclear Magnetic Resonance." *Journal of Orthopaedic Medicine.* 10:1-13. 1992.

48. Magin, R.L., Webb, A.G. and Peck, T.L. "Miniature Magnetic Resonance Machines." *IEEE Spectrum.* 34.10:51-61. 1997.

49. Malemud, C.J. "Changes in Proteoglycans in Osteoarthritis: Biochemistry, Ultrastructure and Biosynthetic Processing." *Journal of Rheumatology.* Volume 18, Supplement 27: 60-62. 1991.

50. Maroudas, A. "Distribution and Diffusion of Solutes in Articular Cartilage." *Biophys. J.* 10:365-379. 1970.

51. Maroudas, A. "Physico-Chemical Properties of Articular Cartilage." In: *Adult Articular Cartilage.* Ed. M.A.R.Freeman. Tunbridge Wells, Kent, England: Pitman Medical. pp. 215-290. 1979.

52. Maroudas, A. and Evans, H. "A Study of Ionic Equilibria in Cartilage." *Connective Tissue Research.* 1:69-77. 1972.

53. Maroudas, A. and Thomas, H. "A Simple Physiochemical Micromethod for Determining Fixed Anionic Groups in Connective Tissue." *Biochim. Biophys. Acta.* 215:214-216. 1970.

54. Maroudas, A. et al. "The Distributions and Diffusivities of Small Ions in Chondroitin Sulfate, Hyaluronate, and some Proteoglycan Solutions." *Biophysical Chemistry.* 32:257-270. 1988.

55. Maroudas, A., Schneiderman, R. and Popper, O. "The Role of Water, Proteoglycan, and Collagen in Solute Transport in Cartilage." In: *Articular Cartilage and Osteoarthritis.* Ed. K. Kuettner et al. New York: Raven Press, Ltd. 1992.

56. Maughan, D.W. and Godt, R.E. "Equilibrium Distribution of Ions in a Muscle Fiber." *Biophys. J.* 56:717-722. 1989.

57. Mezrich, Reuben. "A Perspective on K-Space." *Radiology.* 195:297-315. 1995.

58. Minas, T. and Nehrer, S. "Current Concepts in the Treatment of Articular Cartilage." *Orthopedics.* 20:525-538. 1997.

59. Mitchell, D.G. "MR Imaging Contrast Agent – What's in a Name?" *Journal of Magnetic Resonance Imaging.* 7:1-4. 1997.

60. Narayana, P.A., Kulkarni, M.V. and Mehta, S.D. "NMR of ^{23}Na in Biological Systems." In: *Magnetic Resonance Imaging.* Ed. Partain, C.L. et al. Philadelphia: Saunders. pp. 1553-1563. 1988.

61. Parker, K.H., Winlove, C.P. and Maroudas, A. "The Theoretical Distributions and Diffusivities of Small Ions in Chondroitin Sulfate and Hyaluronate." *Biophysical Chemistry.* 32:271-282. 1988.

62. Paul, P.K. et al. "Detection of Cartilage Degradation with Sodium NMR." *British Journal of Rheumatology.* 30.4:318.

63. Paul, P.K. et al. "Magnetic Resonance Imaging Reflects Cartilage Proteoglycan Degradation in the Rabbit Knee." *Skeletal Radiology.* 20:31-36. 1991.

64. Peyron, J.G. "Is Osteoarthritis a Preventable Disease?" *Journal of Rheumatology.* Volume 18, Supplement 27: 2-3. 1991.

65. Preston, B.N., Snowden, McK. and Houghton,K.T. "Model Connective Tissue Systems: The Effect of Proteoglycans on the Distributions of Small Non-Electrolytes and Micro-Ions." *Biopolymers.* 11:1645-1659. 1972

66. Price, R.R., Stephens, W.H. and Partain, C.L. "NMR Physical Principles." In: *Magnetic Resonance Imaging.* Ed. Partain, C.L. et al. Philadelphia: Saunders. pp. 971-986. 1988.

67. Rajan, S.S. *MRI: A Conceptual Overview.* New York: Springer-Verlag. 1998.

68. Schirra, H.J. "Theory of NMR Spectroscopy." WWW Site: http://www.biochemtech.uni-halle.de/PPS2/projects/schirra/html/theory.htm. Martin-Luther University Halle-Wittenburg. Halle, Saale, Germany. 1996.

69. Schlaikjer, M. and Kolenda, T. "Magnetic Resonance Imaging." WWW Site: http://www.gbar.dtu.dk/~c918480/projekt. Technical University of Denmark. Lyngby, Denmark.

70. Sebastiani, G. and Barone, P. "Mathematical Principles of Basic Magnetic Resonance Imaging in Medicine." *Signal Processing.* 25:227-250. 1991.

71. Tyler, J.A. In: *Cartilage: Molecular Aspects.* Ed. B.K.Hall and S.A.Newman. Boston: CRC Press. pp. 213-356. 1991.

72. Venn, M. and Maroudas, A. "Chemical Composition and Swelling of Normal and Osteoarthrotic Femoral Head Cartilage." *Annals of Rheumatic Diseases.* 36:121-129. 1977.

73. Watson, A.D., Rocklage, S.M. and Carvlin, M.J. "Contrast Agents." In: *Magnetic Resonance Imaging.* 2nd edition. Ed. David D. Stark and William G. Bradley. Boston: Mosby Year Book. pp. 372-437. 1992.

74. Wehrli, F.W. "Principles of Magnetic Resonance." In: *Magnetic Resonance Imaging.* 2nd Edition. Ed. David D. Stark and William G. Bradley. Boston: Mosby Year Book. pp. 3-20. 1992.

75. Wehrli, Felix. "The Origins and Future of Nuclear Magnetic Resonance Imaging." *Physics Today.* 45:34-42. 1992.

76. Willcott, M.R. "NMR Chemical Principles." In: *Magnetic Resonance Imaging.* Ed. Partain, C.L. et al. Philadelphia: Saunders. pp. 987-1002. 1988.

77. Yelin, E. "Arthritis: The Cumulative Impact of a Common Chronic Condition." *Arthritis and Rheumatism.* 35:489-497. 1992.

78. Young, Stuart W. *Magnetic Resonance Imaging Basic Principles.* 2nd edition. New York: Raven Press. 1988.